

## SYNCHROTRON X-RAY-FLUORESCENCE AND LASER-ABLATION ICP-MS MICROPROBES: USEFUL INSTRUMENTS FOR ANALYSIS OF EXPERIMENTAL RUN-PRODUCTS

CLAUDE DALPÉ AND DON R. BAKER

Department of Earth and Planetary Sciences, McGill University, 3450 University Street, Montreal, Quebec H3A 2A7

STEVE R. SUTTON

Department of the Geophysical Sciences and Center for Advanced Radiation Sources (CARS),  
The University of Chicago, Chicago, Illinois 60637, U.S.A.,  
and Department of Applied Sciences, Brookhaven National Laboratory (BNL),  
National Synchrotron Light Source, Upton, New York 11973, U.S.A.

### ABSTRACT

The synchrotron X-ray-fluorescence microprobe (SXRFM) and laser-ablation microprobe with inductively coupled plasma – mass spectrometer (LAM-ICP-MS) have been found to be efficient instruments for the accurate measurement of a large suite of trace elements in natural and synthetic minerals and glasses. The small beam-sizes of both instruments (10 and 34  $\mu\text{m}$  in diameter for SXRFM and LAM-ICP-MS, respectively) permit *in situ* analysis of samples whose cross-section is at least 7500  $\mu\text{m}^2$  (*i.e.*, corresponding to a sampling area of  $50 \times 150 \mu\text{m}$  analyzed by LAM-ICP-MS in rastered grid). This sampling technique applied to LAM-ICP-MS avoids sample damage and minimizes the depth of penetration by the laser using a single hole. Optimization of both instruments was carried out using two in-house basaltic glass standards. The lower limits of detection of the SXRFM for Rb, Sr, Y, Zr, and Nb are approximately 5.5 ppm or less, based upon our in-house standards, and the analyses have an associated precision of  $\pm 20\%$  relative. The lower limits of detection of the LAM-ICP-MS are approximately 2 ppm or less; these analyses have a precision of  $\pm 10$  to 15% relative. Both instruments were used to measure partition coefficients between a Ti-rich calcic amphibole and a Ti-rich basaltic quenched glass produced experimentally. The  $D$  values determined by SXRFM for Sr, Y, and Zr are:  $D_{\text{Sr}}$  0.32 ( $\pm 0.04$ ),  $D_{\text{Y}}$  0.25 ( $\pm 0.04$ ),  $D_{\text{Zr}}$  0.12 ( $\pm 0.07$ ). Partition coefficients determined by LAM-ICP-MS are:  $D_{\text{Rb}}$  0.22 ( $\pm 0.04$ ),  $D_{\text{Sr}}$  0.38 ( $\pm 0.01$ ),  $D_{\text{Y}}$  0.33 ( $\pm 0.03$ ),  $D_{\text{Zr}}$  0.12 ( $\pm 0.01$ ),  $D_{\text{Nb}}$  0.05 ( $\pm 0.01$ ). The LAM-ICP-MS was also used to measure the  $D$  values for Ba, Ta, La, Ce, Nd, Hf, Sm, and Eu, which are:  $D_{\text{Ba}}$  0.28 ( $\pm 0.01$ ),  $D_{\text{Ta}}$  0.07 ( $\pm 0.02$ ),  $D_{\text{La}}$  0.039 ( $\pm 0.005$ ),  $D_{\text{Ce}}$  0.067 ( $\pm 0.002$ ),  $D_{\text{Nd}}$  0.14 ( $\pm 0.01$ ),  $D_{\text{Hf}}$  0.33 ( $\pm 0.01$ ),  $D_{\text{Sm}}$  0.19 ( $\pm 0.08$ ), and  $D_{\text{Eu}}$  0.35 ( $\pm 0.02$ ).

**Keyword:** synchrotron X-ray-fluorescence microprobe, SXRFM, laser-ablation microprobe – inductively coupled plasma – mass spectrometer, LAM-ICP-MS, partition coefficient, pargasite.

### SOMMAIRE

La microsonde à fluorescence X générée par synchrotron (SXRFM) et la microsonde par ablation au laser intégrée à un plasma à couplage inductif avec spectromètre de masse (LAM-ICP-MS) sont reconnues comme instruments analytiques efficaces. Ils permettent une mesure précise d'une suite imposante d'éléments traces dans les verres et minéraux naturels et synthétiques. Les deux instruments ont la propriété d'avoir un petit faisceau (10 et 34  $\mu\text{m}$  de diamètre pour SXRFM et LAM-ICP-MS, respectivement) et ainsi de permettre des analyses *in situ* des échantillons dont la superficie est d'au moins 7500  $\mu\text{m}^2$  (*i.e.*, correspondant à une surface échantillonnée par balayage de  $50 \times 150 \mu\text{m}$  avec le LAM-ICP-MS). L'optimisation des deux microsondes a été pratiquée sur deux étalons de composition basaltique préparés en laboratoire. Le seuil de détection inférieur fondé sur l'analyse de nos étalons internes pour la SXRFM est de l'ordre de 5.5 ppm ou moins pour Rb, Sr, Y, Zr, Nb et d'une précision analytique relative de  $\pm 20\%$ . Le seuil de détection pour le LAM-ICP-MS est de l'ordre de 2 ppm ou moins, avec une précision analytique relative de  $\pm 10$  à 15%. Les deux instruments analytiques ont été utilisés afin de mesurer les valeurs des coefficients de partage dans des produits d'expérience entre une amphibole calcique enrichie en titane et un verre de composition basaltique également enrichi en titane. Les valeurs  $D$  déterminés par SXRFM pour Sr, Y et Zr sont:  $D_{\text{Sr}}$  0.32 ( $\pm 0.04$ ),  $D_{\text{Y}}$  0.25 ( $\pm 0.04$ ),  $D_{\text{Zr}}$  0.12 ( $\pm 0.07$ ). Les coefficients de partage déterminés par LAM-ICP-MS sont:  $D_{\text{Rb}}$  0.22 ( $\pm 0.04$ ),  $D_{\text{Sr}}$  0.38 ( $\pm 0.01$ ),  $D_{\text{Y}}$  0.33 ( $\pm 0.03$ ),  $D_{\text{Zr}}$  0.12 ( $\pm 0.01$ ),  $D_{\text{Nb}}$  0.05 ( $\pm 0.01$ ). Le LAM-ICP-MS a également été utilisé pour mesurer les valeurs  $D$  des éléments Ba, Ta, La, Ce, Nd, Hf, Sm et Eu, qui sont:  $D_{\text{Ba}}$  0.28 ( $\pm 0.01$ ),  $D_{\text{Ta}}$  0.07 ( $\pm 0.02$ ),  $D_{\text{La}}$  0.039 ( $\pm 0.005$ ),  $D_{\text{Ce}}$  0.067 ( $\pm 0.002$ ),  $D_{\text{Nd}}$  0.14 ( $\pm 0.01$ ),  $D_{\text{Hf}}$  0.33 ( $\pm 0.01$ ),  $D_{\text{Sm}}$  0.19 ( $\pm 0.08$ ), and  $D_{\text{Eu}}$  0.35 ( $\pm 0.02$ ).

**Mots-clés:** microsonde à fluorescence X générée par synchrotron, SXRFM, microsonde par ablation au laser intégrée à un plasma à couplage inductif avec spectromètre de masse, LAM-ICP-MS, coefficients de partage, pargasite.

## INTRODUCTION

Trace elements provide a powerful tool for the investigation of the petrogenesis of igneous rocks. Using trace-element concentrations in a suite of rock samples, one can construct an inverse model that not only constrains the mechanisms responsible for the genesis of the suite but also can provide information on the source region (*e.g.*, Allègre *et al.* 1977, Allègre & Minster 1978, Hofmann 1986). These models depend upon accurately characterized partition coefficients (*D*) between minerals and melts. Most of these partition coefficients are based upon analyses of natural phenocrysts and their enclosing glassy matrix. However, because partition coefficients are sensitive to pressure, temperature, and compositions of mineral and melt (including volatile content and oxygen fugacity), they are best measured in minerals and quenched glasses synthesized in the laboratory under controlled conditions.

Electron-microprobe analysis (EMPA) can be used to measure partition coefficients of major and minor elements in glasses and crystals from experimental run-products, but EMPA cannot be used for trace elements (<100 ppm). Furthermore, because of the small size of such run products, minerals and quenched glasses only rarely can be separated by magnetic or density techniques for traditional analytical techniques used on natural rocks and minerals (Watson *et al.* 1987). To determine partition coefficients accurately in experimental run-products, these must be analyzed *in situ* for trace elements using a microbeam technique.

Two microbeam instruments, the synchrotron X-ray fluorescence microprobe (SXRFM) and the laser-ablation microprobe used in conjunction with an inductively coupled plasma – mass spectrometer (LAM-ICP-MS), recently have been used to measure partition coefficients between crystal and glass in experimental run-products (Dalpé *et al.* 1992, Dalpé & Baker 1994a, b, Jenner *et al.* 1993, Skulski *et al.* 1994). Both instruments are rapid and have a lower limit of detection (LLD) near, or below, 5 ppm. These instruments also have been applied to other studies requiring *in situ* analysis (Sutton *et al.* 1987, Jackson *et al.* 1992, Pearce *et al.* 1992, Federowich *et al.* 1993, Feng *et al.* 1993, Feng 1994). In addition, other microbeam instruments have been used for *in situ* analysis as discussed by Hawthorne (1993) and Green (1994).

The two instruments utilized here are based on different principles and have different analytical characteristics, such as sensitivity, stability, interference, and beam size (Gordon 1982, Bos *et al.* 1984, Jones *et al.* 1984, Sutton *et al.* 1986, Lu *et al.* 1989, Jarvis *et al.* 1992, Jarvis & Williams 1993, Perkins *et al.* 1993). Synchrotron radiation is intense, white light of X-ray wavelengths, more than 105 times more brilliant than that of conventional X-ray tubes, emitted from electrons circling a synchrotron ring. As the

specimen is excited by synchrotron X-ray radiation, the SXRFM measures the energies and intensities of X rays emitted by the sample with either an energy-dispersion or wavelength-dispersion detector. Quantification of the elemental concentrations based on the XRF spectrum is relatively straightforward because the physics of photon interactions with matter is well understood. With the SXRFM, one can analyze geological specimens for trace elements in a non-destructive way. The lower limit of detection is 1–10 ppm for a spot size of 10 µm, depending on the element and the matrix analyzed (Sutton *et al.* 1986, Bajt *et al.* 1992).

The recent refinement of the laser-ablation technique for ICP-MS analysis allows microsampling and rapid analysis of materials as different as silicate glass, pressed pellets of rocks, minerals, alloys, and ceramics (Jarvis *et al.* 1992). The LAM ablates a small volume of the sample, some of which is converted into an aerosol and is carried out of the sample cell by argon gas to the inductively coupled plasma (ICP) unit. Inside the ICP, the sample is volatilized, atomized, and ionized; the resulting material undergoes supersonic expansion and is introduced into a quadrupole mass spectrometer (Jarvis *et al.* 1992). Ions are separated from one another by difference in kinetic energies related to their specific mass, and the abundance of selected stable isotopes of trace elements is detected with a Channeltron electron multiplier (Jarvis *et al.* 1992). Advantages of laser-ablation ICP-MS analysis include low LLD, 2 ppm down to hundreds of ppb, speed of analysis, and the ease of sample preparation.

In this paper, we compare these two microprobe techniques in terms of their ability to accurately and precisely analyze two different in-house basaltic glass standards. Then we apply the techniques developed to measure partition coefficients of Rb, Sr, Y, Zr, and Nb between a Ti-rich calcic amphibole and a Ti-rich basaltic quenched glass produced from natural starting materials at 1.5 GPa and 1100°C. These techniques are also applicable to the analysis of other solid experimental run-products and small samples of silicate.

## PREPARATION OF IN-HOUSE STANDARD MATERIALS

Two natural materials were used for optimization of analytical techniques and as in-house standards for analysis of run products. The first material, P-MT, was made from pargasite megacrysts from a lamprophyre dike of Cretaceous age located in the eastern part of the Island of Montréal, Québec. The second material, HF-13, consists of olivine nephelinite from a Tertiary intrusion located in the Mount Llangorse alkaline volcanic field of northern British Columbia (Francis & Ludden 1995).

The pargasite megacrysts are euhedral, up to 5 cm in length. They contain veins of white material along

some cleavage surfaces; we presume that this material consists of calcite + zeolite + anorthoclase, which has been noted in similar megacrysts (Campbell & Schenk 1950, Wallace 1977). The pargasite megacrysts were first coarsely crushed in a steel percussion mortar, and clean chips free of the white material were hand-picked. These chips were ground to a powder (<500 μm) in an agate mortar. The olivine nephelinite was received as powder (<140 μm) prepared in a tungsten carbide ball mill. It is well known that this type of mill can cause contamination in W, Co, Sc, Ta and, possibly, Nb (Hickson & Juras 1986).

Powders of each material were melted four times at 1400°C in an Fe-treated Pt crucible at 1 atmosphere under a controlled oxygen fugacity equal to that of the Fe<sub>2</sub>SiO<sub>4</sub>-Fe<sub>3</sub>O<sub>4</sub>-SiO<sub>2</sub> (FMQ) buffer. The duration of each melting was three hours. Controlled oxygen fugacity was used to prevent the crystallization of opaque phases during melting, which is essential to make a homogeneous glass. After each melting, we obtained a clear brown glass free of crystalline material; this glass was crushed using a steel percussion mortar (to <2 mm in size) and cleaned with a magnet to remove any steel filings from the mortar. After the final melting, the glass was removed from the crucible and crushed into chips up to 3 mm across and magnetically cleaned.

ANALYSIS OF THE IN-HOUSE STANDARD GLASSES FOR MAJOR AND MINOR ELEMENTS

These reference glasses were analyzed for major and minor elements with a JEOL 8900 electron microprobe operated at an accelerating potential of 15 kV with a beam current of 10 nA; for each element, counting times were 25 s on the peak and 10 s on each background position. The beam size was chosen to be the same diameter as the beam size of the SXRFM (i.e., 10 μm). Albite (Na), diopside (Si, Ca, Mg), andradite (Fe), orthoclase (K, Al), and pyrophanite (Mn, Ti) were used as standards. We have checked the homogeneity of the synthesized glasses by analyzing different chips of glass (3-4 mm in size) from the top, middle, and bottom of the crucible (Table 1). Boyd's homogeneity index was used to characterize the homogeneity in major elements of both glasses (Boyd & Finger 1975). On the basis of the standard deviation expected from counting statistics, σ<sub>c</sub>, and the standard deviation associated with data measured on the sample, σ, Boyd & Finger (1975) suggested that a sigma ratio σ/σ<sub>c</sub> in excess of 2-3 for a major element "is highly suggestive of the presence of an inhomogeneity" in the material. All major elements from the three subsamples of P-MT glass have sigma ratios less than 1.5, with a maximum of 1.32 calculated for Si at the top position (Table 1). Because manganese is not a major element, high values were calculated in all three positions, and Boyd's homogeneity test could not be applied. Major

TABLE 1. HOMOGENEITY TEST USING BOYD'S INDEX CALCULATED FROM TOP, MIDDLE, AND BOTTOM CHIPS INSIDE THE CRUCIBLE FOR P-MT AND HF-13 GLASSES

| P-MT Glass                                  |                    |                           |        |              |        |              |
|---|--------------------|---------------------------|--------|--------------|--------|--------------|
| n   | Top                |                           | Middle |              | Bottom |              |
|   | IO                 | Boyd's index <sup>1</sup> | IO     | Boyd's index | IO     | Boyd's index |
| SiO <sub>2</sub>                            | 40.64              | (0.19) 1.32               | 40.47  | (0.12) 0.82  | 40.16  | (0.14) 0.97  |
| TiO <sub>2</sub>                            | 3.82               | (0.04) 0.91               | 3.82   | (0.03) 0.68  | 3.80   | (0.05) 1.19  |
| Al <sub>2</sub> O <sub>3</sub>              | 14.81              | (0.10) 1.17               | 14.79  | (0.07) 0.80  | 14.71  | (0.06) 0.69  |
| <sup>2</sup> Fe <sub>2</sub> O <sub>3</sub> | 1.53               |                           | 1.57   |              | 1.58   |              |
| <sup>2</sup> FeO                            | 7.24               |                           | 7.40   |              | 7.46   |              |
| <sup>3</sup> FeO <sub>T</sub>               | 8.62               | (0.15) 1.30               | 8.81   | (0.10) 0.87  | 8.88   | (0.09) 0.79  |
| MnO   | 0.08               | (0.03) 2.81               | 0.08   | (0.03) 3.08  | 0.10   | (0.02) 2.16  |
| MgO   | 14.44              | (0.11) 1.16               | 14.52  | (0.05) 0.55  | 14.46  | (0.06) 0.66  |
| CaO   | 12.30              | (0.06) 0.78               | 12.34  | (0.06) 0.67  | 12.36  | (0.05) 0.61  |
| Na <sub>2</sub> O                           | 1.92               | (0.03) 0.80               | 1.92   | (0.03) 0.80  | 1.91   | (0.03) 0.83  |
| K <sub>2</sub> O                            | 2.31               | (0.03) 0.93               | 2.28   | (0.03) 1.01  | 2.28   | (0.03) 1.03  |
| P <sub>2</sub> O <sub>5</sub>               | 0.04               | (0.02) n.d.               | 0.04   | (0.02) n.d.  | 0.04   | (0.02) n.d.  |
| Total                                       | 98.98 <sup>4</sup> |                           | 99.07  |              | 98.70  |              |

| HF-13 Glass                                 |                    |              |        |              |        |              |
|---|--------------------|--------------|--------|--------------|--------|--------------|
| n   | Top                |              | Middle |              | Bottom |              |
|   | IO                 | Boyd's index | IO     | Boyd's index | IO     | Boyd's index |
| SiO <sub>2</sub>                            | 41.24              | (0.21) 1.43  | 41.43  | (0.11) 0.74  | 41.64  | (0.17) 1.12  |
| TiO <sub>2</sub>                            | 2.45               | (0.03) 0.96  | 2.47   | (0.03) 1.04  | 2.45   | (0.02) 0.76  |
| Al <sub>2</sub> O <sub>3</sub>              | 11.61              | (0.06) 0.86  | 11.63  | (0.05) 0.73  | 11.49  | (0.10) 1.37  |
| <sup>2</sup> Fe <sub>2</sub> O <sub>3</sub> | 2.32               |              | 2.31   |              | 2.30   |              |
| <sup>2</sup> FeO                            | 10.17              |              | 10.16  |              | 10.11  |              |
| <sup>3</sup> FeO <sub>T</sub>               | 12.26              | (0.14) 0.96  | 12.24  | (0.23) 1.57  | 12.18  | (0.17) 1.19  |
| MnO   | 0.24               | (0.02) 1.34  | 0.22   | (0.03) 1.68  | 0.23   | (0.03) 1.66  |
| MgO   | 11.36              | (0.04) 0.56  | 11.37  | (0.05) 0.65  | 11.34  | (0.08) 0.97  |
| CaO   | 11.01              | (0.07) 0.90  | 11.02  | (0.07) 0.91  | 11.04  | (0.06) 0.82  |
| Na <sub>2</sub> O                           | 5.12               | (0.04) 0.63  | 5.13   | (0.06) 0.98  | 5.11   | (0.04) 0.71  |
| K <sub>2</sub> O                            | 2.02               | (0.03) 0.90  | 2.00   | (0.03) 0.89  | 2.01   | (0.02) 0.76  |
| P <sub>2</sub> O <sub>5</sub>               | 1.46               | (0.03) n.d.  | 1.46   | (0.03) n.d.  | 1.46   | (0.03) n.d.  |
| Total                                       | 98.77 <sup>4</sup> |              | 98.97  |              | 98.95  |              |

Concentrations are in weight percent (wt%).  
<sup>1</sup>: Boyd's index is calculated using the relationship  $\sigma / \sigma_c$ , where  $\sigma$  is the measured standard deviation from electron probe in the sample and  $\sigma_c$  is expressed by the following equation:  $\sigma_c = C / R * [(R * c) / (C * t) + (R * c^2) / (T * C^2)]^{1/2}$  where: C = concentration of an element in the standard; c = concentration of an element in the sample; R = counting rates on the standard (= N / T); N = total counts on the standard; T = counting time on the standard; t = counting time on the sample (Boyd & Finger 1975).  
<sup>2</sup>: Fe<sub>2</sub>O<sub>3</sub> and FeO proportions are calculated using total iron from the electron probe at T = 1400 °C, P = 1 atm, and f O<sub>2</sub> = FMQ (Kress & Carmichael 1991).  
<sup>3</sup>: Total iron is calculated as FeO from electron probe.  
<sup>4</sup>: Totals are calculated using FeO<sub>T</sub>.  
 n.d.: Not determined.  
 Values in parentheses are based on one standard deviation from multiple analyses (1σ).

elements in HF-13 glass samples displayed sigma ratios less than 2, with a maximum of 1.57 for FeO<sub>T</sub> in the middle subsample. Here too, the test for manganese could not be applied. These low values of the sigma ratio indicate that P-MT and HF-13 glasses are homogeneous in major elements.

ANALYSIS OF IN-HOUSE STANDARD GLASSES BY SOLUTION ICP-MS TECHNIQUES

Two grams of each glass (mixtures from the top, middle, and bottom of the crucible) were ground to a

TABLE 2a. IN-HOUSE GLASS STANDARD COMPOSITIONS (MAJOR AND MINOR ELEMENTS)

| Ref. Glass comp.                             | P-MT Glass Pargasitic |        | HF-13 Glass Ol-normative nephelinitic |        |
|--|-----------------------|--------|---------------------------------------|--------|
|  | 30                    |        | 30                                    |        |
| SiO <sub>2</sub>                             | 40.43                 | (0.25) | 41.44                                 | (0.24) |
| TiO <sub>2</sub>                             | 3.81                  | (0.04) | 2.46                                  | (0.03) |
| Al <sub>2</sub> O <sub>3</sub>               | 14.77                 | (0.09) | 11.58                                 | (0.10) |
| <sup>56</sup> Fe <sub>2</sub> O <sub>3</sub> | 1.56                  |        | 2.31                                  |        |
| <sup>54</sup> FeO                            | 7.37                  |        | 10.15                                 |        |
| <sup>56</sup> FeO <sub>T</sub>               | 8.77                  | (0.16) | 12.23                                 | (0.18) |
| MnO  | 0.09                  | (0.03) | 0.23                                  | (0.03) |
| MgO  | 14.48                 | (0.09) | 11.36                                 | (0.06) |
| CaO  | 12.34                 | (0.06) | 11.02                                 | (0.07) |
| Na <sub>2</sub> O                            | 1.92                  | (0.03) | 5.12                                  | (0.05) |
| K <sub>2</sub> O                             | 2.29                  | (0.03) | 2.01                                  | (0.03) |
| P <sub>2</sub> O <sub>5</sub>                | 0.04                  | (0.02) | 1.46                                  | (0.03) |
| Total  | 98.94 <sup>3</sup>    |        | 98.91                                 |        |

Concentrations are in weight percent (wt%).

<sup>1</sup>: Fe<sub>2</sub>O<sub>3</sub> and FeO proportions are calculated using total iron from the electron probe at T = 1400 °C, P = 1 atm, and fO<sub>2</sub> = FMQ (Kress & Carmichael 1991).

<sup>2</sup>: Total iron is calculated as FeO from electron probe.

<sup>3</sup>: Totals are calculated using FeO<sub>T</sub>.

powder (<245 μm) in an agate mortar, split into 1-gram aliquots, and sent to two different laboratories (Memorial University of Newfoundland and Université de Montréal) for analysis by solution ICP-MS techniques. Table 2a shows the concentrations of major and minor elements measured by electron microprobe, and Table 2b shows the concentrations of trace elements measured by solution ICP-MS techniques. The solution ICP-MS analyses performed at Memorial University of Newfoundland used the method of standard addition to correct for matrix effects (Jenner *et al.* 1990, Longerich *et al.* 1990); at the Université de Montréal, a method of calibration based on matrix-matched external standardization and nonlinear response drift-corrections was used (Cheatham *et al.* 1993). The composition of the original HF-13 bulk rock before melting, analyzed by three different techniques, also is listed in Table 2b. This composition was recalculated on an anhydrous basis for comparison with the actual glass composition after melting. At the two-sigma level for most elements, no systematic difference appears between the original composition and the results of solution-mode ICP-MS analyses of the HF-13 glass after melting (Table 2b). The only exceptions are Ta, La, and Eu, whose concentrations are higher than those reported in the original bulk-rock analysis. Comparison of the results of different ICP-MS analyses of in-house glass standards from both laboratories demonstrate that they are in very good agreement for the majority of elements, with the exception of Y, Nb, Ba, Pr, Nd, and Yb (Table 2b). The concentrations of Nb, Ba, Nd are systematically higher, and those of Y, Pr, Yb, lower, for glasses analyzed at Memorial University of

TABLE 2b. IN-HOUSE GLASS STANDARD COMPOSITIONS (TRACE ELEMENTS)

| Ref. Glass comp. | P-MT Glass Pargasite     |                      | HF-13 Glass Ol-normative nephelinitic |                      | XRF+ICP <sup>2</sup> Before melting |
|------------------|--------------------------|----------------------|---------------------------------------|----------------------|-------------------------------------|
|                  | sol. ICP-MS <sup>1</sup> |                      | sol. ICP-MS                           |                      |                                     |
|                  | UM <sup>3</sup><br>3     | MU <sup>4</sup><br>4 | UM <sup>3</sup><br>2                  | MU <sup>4</sup><br>1 |                                     |
| n                |                          |                      |                                       |                      | 3                                   |
| Li               | n.d.                     | 2.7 (0.5)            | n.d.                                  | 12.40                | n.d.                                |
| Rb               | 16.2 (0.31)              | 16.9 (0.5)           | 29.0                                  | 28.4                 | 29.72 (0.45)                        |
| Sr               | 461.7 (13.4)             | 474.6 (5.20)         | 1532                                  | 1485                 | 1498 (37.6)                         |
| Y                | 12.00 (0.32)             | 9.73 (0.25)          | 30.46                                 | 23.89                | 27.40 (2.28)                        |
| Zr               | 53.08 (1.95)             | 52.35 (1.46)         | 301.9                                 | 292.7                | 299.9 (13.9)                        |
| Nb               | 13.25 (0.89)             | 16.62 (0.38)         | 103.6                                 | 114.6                | 90.78 (7.28)                        |
| Ba               | 360.4 (12.7)             | 365.9 (8.90)         | 320.9                                 | 337.1                | 391.4 (62.4)                        |
| Hf               | 2.14 (0.12)              | 2.35 (0.12)          | 6.05                                  | 6.54                 | 5.99 (0.25)                         |
| Ta               | 0.96 (0.07)              | 1.02 (0.06)          | 5.79                                  | 5.87                 | 4.68 (0.05)                         |
| Pb               | 3.83 (0.17)              | 4.50 (1.06)          | 0.61                                  | 0.45                 | n.d.                                |
| Th               | 0.17 (0.01)              | 0.21 (0.04)          | 9.13                                  | 9.21                 | 9.61 (1.34)                         |
| U                | 0.05 (0.002)             | 0.06 (0.01)          | 2.84                                  | 2.81                 | 2.47 (0.25)                         |
| La               | 5.77 (0.21)              | 5.78 (0.06)          | 82.82                                 | 83.73                | 77.87 (1.19)                        |
| Ce               | 17.01 (0.75)             | 18.07 (0.21)         | 159.18                                | 167.76               | 139 (11)                            |
| Pr               | 3.11 (0.11)              | 2.89 (0.04)          | 20.03                                 | 18.67                | n.d.                                |
| Nd               | 14.53 (0.53)             | 15.31 (0.40)         | 73.35                                 | 76.91                | 67.17 (3.16)                        |
| Sm               | 3.74 (0.15)              | 3.91 (0.23)          | 14.06                                 | 14.42                | 13.85 (0.25)                        |
| Eu               | 1.29 (0.05)              | 1.36 (0.06)          | 4.48                                  | 4.49                 | 4.08 (0.13)                         |
| Gd               | 3.41 (0.16)              | 4.40 (0.31)          | 11.31                                 | 11.76                | 10.88 <sup>5</sup>                  |
| Tb               | 0.48 (0.03)              | 0.52 (0.04)          | 1.53                                  | 1.47                 | 1.40 (0.08)                         |
| Dy               | 2.53 (0.14)              | 2.62 (0.12)          | 6.97                                  | 7.04                 | 6.71 <sup>3</sup>                   |
| Ho               | 0.43 (0.02)              | 0.45 (0.01)          | 1.06                                  | 1.11                 | 1.18 (0.13)                         |
| Er               | 1.08 (0.03)              | 1.05 (0.06)          | 2.72                                  | 2.45                 | n.d.                                |
| Tm               | 0.13 (0.01)              | 0.12 (0.01)          | 0.30                                  | 0.27                 | 0.27 <sup>3</sup>                   |
| Yb               | 0.73 (0.05)              | 0.68 (0.01)          | 1.61                                  | 1.38                 | 1.47 (0.02)                         |
| Lu               | 0.10 (0.004)             | 0.09 (0.01)          | 0.20                                  | 0.18                 | 0.20 (0.01)                         |

Concentrations are in parts per million (ppm).

<sup>1</sup>: Analyzed by solution inductively coupled plasma mass spectrometry at respectively laboratories show in table.

<sup>2</sup>: Analyzed by X-ray fluorescence, solution ICP-MS, and irradiation neutron activation (INA) at McGill University and the Université de Montréal before melting the bulk powder to make standard (D. Francis, pers. comm., 1994). Concentrations of trace elements are recalculated on anhydrous basis.

<sup>3</sup>: Analyses done at the Laboratoire Ultratrace du Département de Géologie de l'Université de Montréal by G. Gauthier and A. Khoury.

<sup>4</sup>: Analyses done at the Department of Earth Sciences, Memorial University of Newfoundland by S.E. Jackson.

<sup>5</sup>: Single analysis.

n.d.: Not determined.

Values in parentheses are based on one standard deviation from multiple analyses (1σ). Sample chips from both glasses are available upon request to the first author.

Newfoundland compared to those analyzed at Université de Montréal. Both laboratories use different methods to establish the concentration of those elements. Calibration curves for Y at Université de Montréal are based upon the average values of Y in the standards BIR-1, BHVO-1, JB-1, and BR (Govindaraju 1989), whereas at Memorial University of Newfoundland, a pure Y metal is used for calibration. The Y concentrations obtained by Memorial University of Newfoundland on different international reference materials are reported to be 20% lower than values previously suggested (G. Jenner, pers. comm., 1995). So without any evidence to the contrary, and knowing that both laboratories can reproduce compositions of basaltic reference standards with excellent accuracy using different procedures of calibration (typically better than ±5%; Jenner *et al.* 1990, Cheatham *et al.* 1993), we decided to use the average trace-element concentrations for Rb, Sr, Y, Zr, Nb, Ba,

TABLE 3. LEVELS OF DIFFERENT TRACE ELEMENTS AS DETERMINED BY SXRF AND LASER-ABLATION ICP-MS MICROPROBES

| P-MT Glass              |                                |             |              |                  |
|-------------------------|--------------------------------|-------------|--------------|------------------|
| SXRFM                   |                                |             |              |                  |
|                         | Working <sup>1</sup><br>values | Top         | Middle       | LLD <sup>2</sup> |
| <i>n</i>                |                                | 5           | 5            | 10               |
| Rb                      | 16.6                           | 16.0 (0.89) | 13.6 (0.49)  | 2.90             |
| Sr                      | 469                            | 449 (10.9)  | 359 (3.41)   | 3.26             |
| Y                       | 10.7                           | 10.6 (0.49) | 9.40 (0.80)  | 3.14             |
| Zr                      | 52.7                           | 42.4 (1.50) | 29.2 (0.98)  | 5.08             |
| Nb                      | 15.2                           | 12.4 (1.02) | 10.2 (1.17)  | 5.19             |
| LAM-ICP-MS <sup>2</sup> |                                |             |              |                  |
|                         |                                | Top         | Middle       | LLD              |
| <i>n</i>                |                                | 5           | 5            | 10               |
| Rb                      | 16.6                           | 16.7 (0.21) | 20.08 (0.53) | 0.71             |
| Sr                      | 469                            | 451 (1.94)  | 456 (2.42)   | 0.81             |
| Y                       | 10.7                           | 9.24 (0.32) | 9.75 (0.26)  | 0.86             |
| Zr                      | 52.7                           | 52.4 (0.72) | 53.3 (1.19)  | 1.09             |
| Nb                      | 15.2                           | 13.9 (0.18) | 14.3 (0.29)  | 0.72             |
| Ba                      | 364                            | 407 (1.11)  | 417 (3.71)   | 0.12             |
| La                      | 5.78                           | 5.78 (0.14) | 5.93 (0.12)  | 0.18             |
| Ce                      | 17.6                           | 18.9 (0.32) | 19.3 (0.15)  | 0.11             |
| Nd                      | 14.9                           | 15.8 (0.37) | 16.2 (0.20)  | 0.10             |
| Sm                      | 3.84                           | 4.44 (0.28) | 4.27 (0.35)  | 0.37             |
| Eu                      | 1.33                           | 1.29 (0.09) | 1.35 (0.08)  | 0.09             |
| Hf                      | 2.26                           | 2.49 (0.21) | 2.32 (0.07)  | 0.09             |
| Ta                      | 1.0                            | 1.06 (0.07) | 1.14 (0.05)  | 0.10             |

| HF-13 Glass             |                   |             |             |                  |
|-------------------------|-------------------|-------------|-------------|------------------|
| SXRFM                   |                   |             |             |                  |
|                         | Working<br>values | Top         | Middle      | LLD <sup>2</sup> |
| <i>n</i>                |                   | 5           | 5           | 10               |
| Rb                      | 28.8              | 33.0 (0.89) | 28.6 (1.02) | 2.46             |
| Sr                      | 1516              | 1718 (9.80) | 1432 (65.2) | 2.75             |
| Y                       | 28.3              | 27.4 (0.80) | 23.8 (1.72) | 3.35             |
| Zr                      | 299               | 290 (5.31)  | 229 (14.4)  | 4.97             |
| Nb                      | 107               | 92.6 (2.06) | 74.6 (3.88) | 4.13             |
| LAM-ICP-MS <sup>2</sup> |                   |             |             |                  |
|                         |                   | Top         | Middle      | LLD              |
| <i>n</i>                |                   | 5           | 5           | 10               |
| Rb                      | 28.8              | 33.6 (0.51) | 31.0 (0.61) | 0.65             |
| Sr                      | 1516              | 1506 (5.28) | 1506 (2.45) | 0.65             |
| Y                       | 28.3              | 25.4 (0.41) | 25.3 (0.47) | 0.77             |
| Zr                      | 299               | 316 (2.91)  | 320 (3.11)  | 0.90             |
| Nb                      | 107               | 101 (0.64)  | 101 (1.06)  | 0.66             |
| Ba                      | 326               | 344 (3.83)  | 347 (2.28)  | 0.12             |
| La                      | 83.1              | 87.3 (0.44) | 88.3 (0.84) | 0.19             |
| Ce                      | 162               | 171 (0.65)  | 170 (1.17)  | 0.11             |
| Nd                      | 74.5              | 80.6 (0.85) | 79.8 (1.43) | 0.10             |
| Sm                      | 14.2              | 14.2 (0.85) | 16.0 (0.45) | 0.36             |
| Eu                      | 4.5               | 4.41 (0.08) | 4.60 (0.08) | 0.09             |
| Hf                      | 6.2               | 6.86 (0.18) | 7.06 (0.22) | 0.09             |
| Ta                      | 5.8               | 6.02 (0.10) | 6.38 (0.05) | 0.09             |

<sup>1</sup>: Working values are based on average of solution ICP-MS analyses.

<sup>2</sup>: Analytical masses used are listed in Table 4.

<sup>3</sup>: Lower Limit of Detection are based on 10 different analyses from spots (SXRFM) or grids (LAM-ICP-MS).

Values in parentheses are based on one standard deviation from multiple analyses (1 $\sigma$ ).

## MICROBEAM TRACE-ELEMENT ANALYSIS

## Synchrotron X-ray-fluorescence microprobe

SXRFM analyses were performed on beam line X26A at the National Synchrotron Light Source at Brookhaven National Laboratory (Upton, New York). The synchrotron storage ring was operated at 2584 MeV, with an electron current in the range of 110 to 202 mA. Figure 1 shows a schematic view of the X26A beam line and includes the major devices used during analyses. The X radiation from the synchrotron is reduced to a 10- $\mu$ m beam by a series of collimators (slits) and a final pinhole. The beam intensity is measured in a He-filled ion chamber upstream of the pinhole, and the X-ray fluorescence from the sample is detected by a Si(Li) energy-dispersion spectrometer (EDS) (150 eV resolution at MnK $\alpha$ ) positioned at 90°

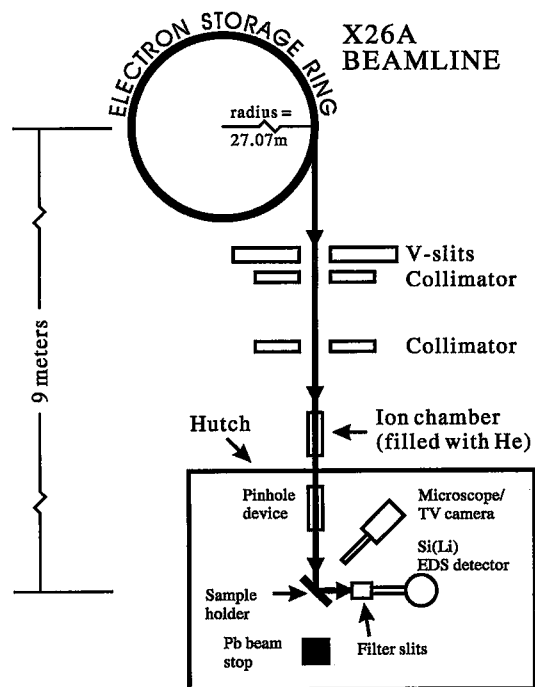


FIG. 1. Schematic view of the X26A beam line at the National Synchrotron Light Source, Brookhaven National Laboratory. The X radiation is emitted from the divergent electrons along their trajectory inside the ring, passes through a series of collimators (slits) and pinhole before exciting the specimen 9 m downstream. The sample is mounted vertically and at 45° to the incident X-ray beam. The fluorescence and scattered X-rays from the specimen are detected with a Si(Li) EDS detector mounted at 90° to the incident beam.

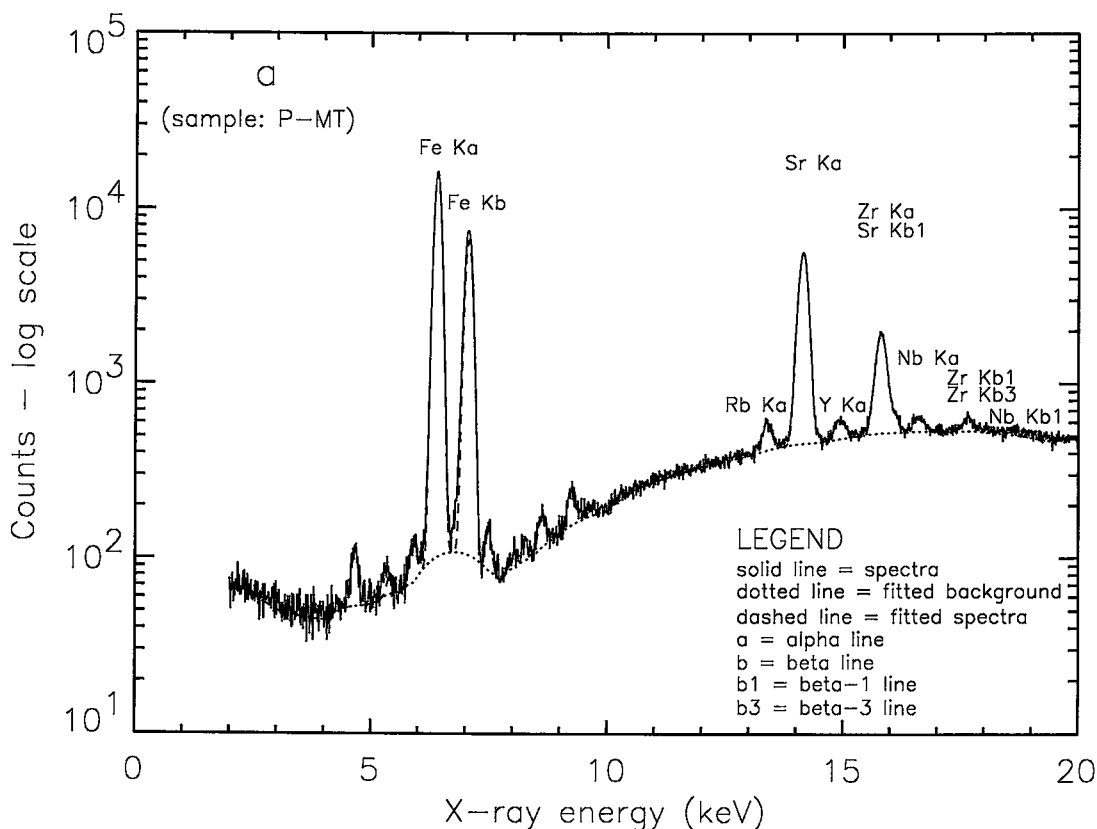
La, Ce, Nd, Sm, Eu, Hf, and Ta determined from the two solution-mode ICP-MS analyses as the working values for the in-house standard glasses HF-13 and P-MT (Table 3). In any case, discrepancies between the different values for Y, Nb, Ba, Pr, Nd, and Yb concentrations will not affect the conclusions of this study.

to the incident beam (Bos *et al.* 1984, Lu *et al.* 1989, Sutton *et al.* 1986). Between the detector and the sample, an aluminum filter either 85 or 170  $\mu\text{m}$  thick (depending upon the sample's composition) is positioned to suppress the intense  $K$  fluorescence lines of major elements, principally Ca and Fe in our samples. Counting dead-time for the EDS detector was maintained in the range of 20 to 30%. Concentrations of trace elements were measured on the same areas previously analyzed by electron microprobe (position located at  $\pm 10 \mu\text{m}$  to the previously analyzed area on the basis of back-scattered electron images). Live time was selected to be 300 s for analyses, yielding a real acquisition time of 390 s. The energy window of the measured spectra was between 2 and 20 keV.

#### Computation of element concentrations and their precision and accuracy

Typical SXRFM spectra of P-MT and HF-13 are shown in Figure 2. The net areas under the peak in each spectrum were obtained by fitting and subtracting a polynomial background, then fitting Gaussian functions to the residual. Trace-element concentrations are based on the technique of internal standard analysis

using a modified version of the program NRLXRF (Sutton *et al.* 1987, Bajt *et al.* 1992). This program calculates concentrations of trace elements with corrections for filters (incident beam and detector filters), major-element composition, self absorption, secondary fluorescence, and the specimen's density and thickness. The thickness of each specimen at the point of analysis was measured with a NIKON binocular microscope at 100 $\times$  and corrected with the material's mean index of refraction to yield the true thickness. The index of refraction of the glasses was measured using immersion oils. Glass densities were calculated using the model of Bottinga *et al.* (1982). Indices of refraction and densities of crystalline phases were estimated using values from Deer *et al.* (1985) for minerals of similar composition. A trace element's concentration is determined by a comparison of the area of the trace element's  $K\alpha$  peak with the area of the  $K\alpha$  peak of an element whose concentration in the sample is known. The internal standard used was iron, previously determined by EMPA at the same point analyzed by SXRFM. The areas of the  $\text{Fe}K\alpha$  peak and trace element's  $K\alpha$  peak were combined with the concentration of iron in the specimen to determine the concentration of a trace element using the relation



$$C_i = S_i \times \frac{I_i}{I_{\text{Fe}}} \times C_{\text{Fe}}$$

in which  $C_i$  is the concentration of a trace element  $i$ ,  $S_i$  is detection sensitivity (ppm/count) for an element  $i$  relative to that for Fe calculated by the NRLXRF program,  $I_i$  represents the integrated counts from element  $i$  ( $K\alpha$  peak),  $I_{\text{Fe}}$  stands for the integrated counts from the  $\text{Fe}K\alpha$  peak, and  $C_{\text{Fe}}$  is the Fe content of the specimen (expressed as the weight fraction of the element; Sutton *et al.* 1987, Lu *et al.* 1989).

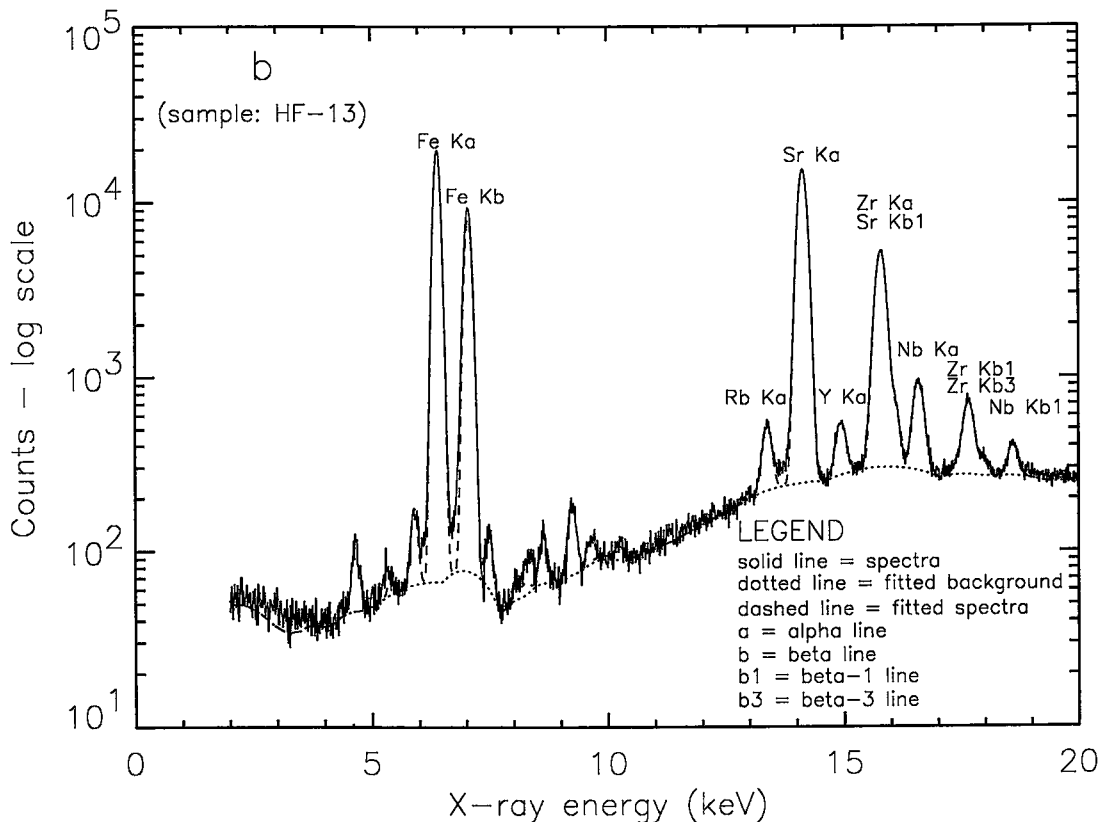
We calculated the effects of errors in thickness, density, and iron content of the specimen on the measured concentrations of the trace elements. An error of  $\pm 10\%$  relative on either the thickness or the density of a specimen produces a maximum error of  $\pm 7\%$  relative in the trace-element concentrations; an error of  $\pm 10\%$  relative in the iron concentration results in a maximum error of  $\pm 10\%$  relative in the trace-element concentrations. Other potential, systematic errors associated with

the SXRFM include uncertainties in the thickness and composition of the filters used between the specimen and the detector (Lu *et al.* 1989). As we show below, by careful analysis, we can analyze our materials for trace elements using SXRFM to accuracies within  $\pm 20\%$  relative of the accepted values, at concentrations in the ppm range.

*Laser-ablation microprobe – inductively coupled plasma – mass spectrometry*

LAM-ICP-MS analyses were performed with a Fisons PQ2+ ICP-MS mass spectrometer equipped with a laser microprobe at the Université de Montréal. The laser is of the Nd:YAG type, operating at a wavelength of 1064 nm. This laser can be used in two modes: “Q-switched” and “free-running”. In the Q-switched mode, laser radiation does not exit the laser cavity until the radiation reaches a critical level of

FIG. 2. Synchrotron X-ray-fluorescence microprobe (SXRFM) spectra showing counts versus X-ray energy. The labeled peaks refer to the principal  $K$ -energy fluorescence lines. (a) Top subsample of HF-13 glass. (b) Top subsample of P-MT glass.



power, which produces a high-power, short-duration pulse (Jarvis *et al.* 1992, Williams & Jarvis 1993). In the free-running mode, all laser radiation exits the laser cavity; this radiation is of lower power than radiation in the Q-switched mode, but is emitted as a relatively long sequence of pulses (Jarvis *et al.* 1992). The Q-switched mode is used routinely at our facility because it is practically impossible to ablate clear glass samples (*e.g.*, NIST-612 standard) using the free-running mode owing to lower overall efficiencies in ablation (Federowich *et al.* 1993).

However, for the analysis of small samples, the free-running mode has the advantage of minimizing damage to the sample. We have measured the ablation rates for both Q-switched and free-running modes on HF-13, P-MT and NIST-612 glasses with a laser blank voltage of 945 V and a repetition rate of 4 Hz. In the present study, the ablation rate of the free-running mode is  $\sim 80 \mu\text{m}/\text{min}$ , whereas in Q-switched mode, the ablation rate is 25% greater,  $\sim 100 \mu\text{m}/\text{min}$ . Furthermore, diameters of the ablation craters are smaller for the free-running than the Q-switched mode, 34 and 62  $\mu\text{m}$ , respectively. The same response in crater diameter between both modes was observed by Williams & Jarvis (1993). Thus the free-running mode is better suited for the analysis of small samples than the Q-switched mode. However, the free-running mode must be used with a colored sample and results in minimum limits of detection that are a factor of 10 to 100 times greater than with the Q-switched mode (discussed below).

TABLE 4. LASER MICROPROBE AND ICP-MS: OPERATING CONDITIONS

|                         |   |
|-------------------------|---|
| <b>Laser Microprobe</b> |   |
| laser mode              | "Free-running"  |
| voltage                 | 945 V   |
| repetition rate         | 4 Hz/4 shots  |
| grid parameters         | matrix of $2 \times 10$ ablation holes (increments of 20 $\mu\text{m}$ along x-axis and 15 $\mu\text{m}$ along y-axis)  |
| total shots per grid    | 80  |
| element menu            | 17 elements including $^{44}\text{Ca}$ as internal standard   |
| size of sampling grid   | $50 \times 150 \times 80$ (L x W x D) $\mu\text{m}^3$   |
| uptake                  | one full grid (25 s/grid)   |
| focus condition         | on sample surface   |
| <b>ICP-MS</b>           |   |
| extraction lens         | -188 to -202 V  |
| collector lens          | 1.36 to 3.4 V   |
| nebulizer flow rate     | 1.144 to 1.192 L/m  |
| cooling gas             | 13.50 to 13.75 L/m  |
| auxiliary gas           | 0.800 to 0.825 L/m  |
| mass resolution         | 0.8 at 10 % peak height   |
| acquisition mode        | peak jumping  |
| measuring point / peak  | 3 points separated by 1/200 AMU <sup>1</sup>  |
| dwelt-time per point    | 10.24 ms/pt   |
| acquisition time        | 45 s  |
| numbers of repeats      | 3 (total time = 135 s)  |
| completed sweep         | 65  |
| total time / mass       | 1.997 s/mass  |
| analytical masses       | $^{44}\text{Ca}$ , $^{87}\text{Rb}$ , $^{88}\text{Sr}$ , $^{89}\text{Y}$ , $^{90}\text{Zr}$ , $^{93}\text{Nb}$ , $^{137}\text{Ba}$ , $^{139}\text{La}$ , $^{140}\text{Ce}$ , $^{141}\text{Pr}$ , $^{146}\text{Nd}$ , $^{147}\text{Sm}$ , $^{151}\text{Eu}$ , $^{178}\text{Hf}$ , $^{181}\text{Ta}$ , $^{232}\text{Th}$ , $^{238}\text{U}$ |

<sup>1</sup> : Atomic mass unit.

The specimen was ablated inside a silica-glass sample cell under a microscope, with the laser in the free-running mode at a 945 V blank voltage and repetition frequency of 4 Hz. The parameters used for analysis in the free-running mode are listed in Table 4. To minimize damage, the specimen was rastered during ablation and analysis. Each analysis results from a  $2 \times 10$  matrix of ablation holes, which corresponds to a volume of  $50 \times 150 \times 80$  (L x W x D)  $\mu\text{m}^3$  (Fig. 3). This mode results in relatively little damage to the anhydrous and hydrous samples, but cannot be used where elements have abundances below  $\sim 0.1$  ppm (Table 3). The ablated material from the sample cell was transferred to the ICP-MS torch *via* a polyurethane tube of 3 mm (i.d.) over a distance of approximately 1.5 m by a continuously flowing stream of Ar gas at atmospheric pressure.

#### Protocol used during the LAM-ICP-MS analyses

The protocol followed during the analyses begins with a gas blank to establish the instrument's background levels, three analyses of our HF-13 in-house glass standard for external calibration, another gas blank, and then five unknowns. For our purpose, we repeated that protocol twice to analyze a total of 10 unknowns in 1.5 h. Prior to data collection for every analysis of the in-house standard and unknowns, the sample was ablated with the laser for 1.25 s at each of the 20 points of the grid (Fig. 3a); this procedure removed the sample's surface (to a depth of  $\sim 34 \mu\text{m}$ ) and any contaminants adhering to it. Between each analysis, a pause of one minute served to flush the gas line between the sample cell and the ICP-MS unit, and also to allow the mass spectrometer to stabilize at background levels.

The acquisition time for one complete analysis was fixed at three repetitions of 45 s each on the same grid for a total time of 135 s (Table 4). In this way, each analysis represents  $\sim 22$  laser shots in each of the 20 holes made in the  $2 \times 10$  grid. For a typical menu of 17 isotopes, the total time spent on each mass during one complete analysis is approximately 2 s. The internal standard used was  $^{44}\text{Ca}$  because it successfully reproduces trace-element concentrations of P-MT and HF-13 glasses within a relative difference of  $\pm 15\%$  compared to the solution-mode results obtained on the HF-13 in-house glass standard.

#### Computation of element concentrations and their precision and accuracy

Trace-element concentrations were calculated from the measured count-rates for each isotope by comparing the average background-corrected ablation values of the specimen to an in-house basaltic glass standard (HF-13). As mentioned previously, basaltic glass was used instead of NIST glasses because the Nd:YAG

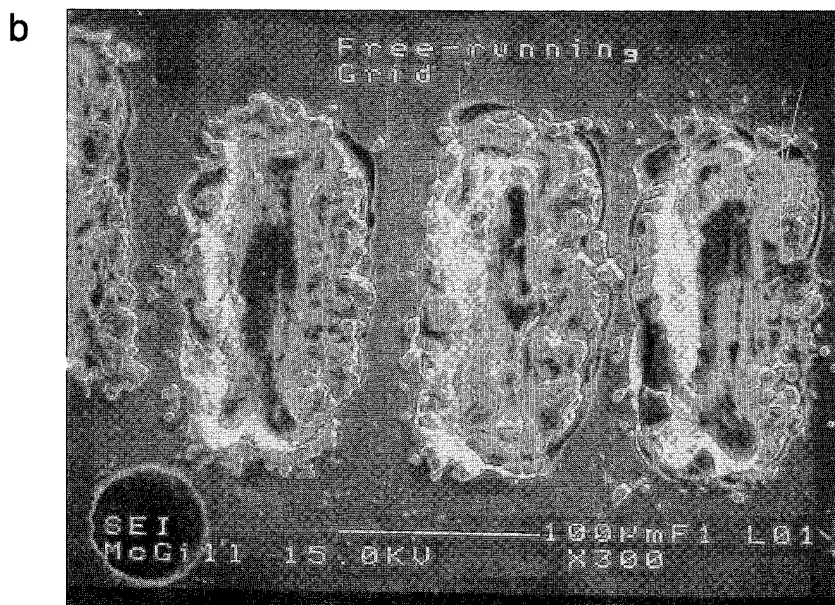
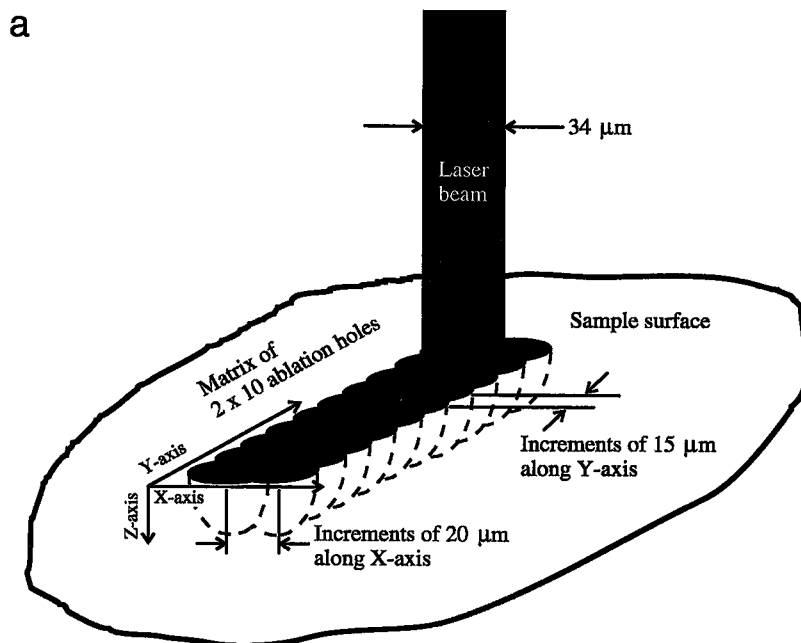


FIG. 3. Physical characteristics of the laser-ablation rastered grid. (a) Schematic view of the ablation-grid pattern. (b) Back-scattered electron images of anhydrous glass (HF-13) showing top view of rastered grid produced in "free-running" mode at operating conditions shown in Table 4 (scale bar: 100  $\mu\text{m}$ ).

laser does not inductively couple with transparent glasses in the free-running mode at the conditions used (Table 4). Concentrations were calculated with the relation:

$$C_{elem, unk} = \frac{\left( \frac{Cps_{isotope}}{Cps_{Ca}} \right)_{unk} \times \frac{CaO_{unk}}{CaO_{stand}}}{\left( \frac{Cps_{isotope}}{Cps_{Ca}} \right)_{stand}} \times C_{elem, stand}$$

where  $C_{elem, unk}$  stands for the calculated concentration of a particular element in the unknown sample (in oxide wt%, ppm, ppb, etc.),  $Cps_{isotope}$  represents the background-corrected counts per second of a particular isotope,  $Cps_{Ca}$  represents the background-corrected counts per second of the internal standard reference isotope,  $^{44}\text{Ca}$ ,  $unk$  is the unknown sample,  $stand$  is the in-house standard sample,  $CaO_{unk}$  is the CaO content in the unknown sample analyzed by EMPA or other analytical techniques (in oxide wt%),  $CaO_{stand}$  is the

CaO content in the in-house standard sample analyzed by EMPA or other analytical techniques (in oxide wt%), and  $C_{elem, stand}$  is the concentration of the element in the in-house standard analyzed previously by EMPA or other analytical techniques (in oxide wt%, ppm, ppb, etc.).

An error of  $\pm 10\%$  relative in the Ca concentration measured by the EMPA on both materials (*i.e.*, CaO determined in unknown and in-house standard) results in a maximum error of  $\pm 20\%$  relative for all the elements analyzed with the LAM-ICP-MS using the above formula. This error is similar to that for the SXRFM. Other variables associated with the instrument and the specimen will affect both precision and accuracy: focusing below the surface of the specimen, differences in total abundance of rare-earth elements (*REE*) between the standard and specimen, thermal fractionation between the internal isotope and the isotopes monitored during ablation, irregular rate of sampling during the ablation owing to physical weakness (*e.g.*, internal fractures in glass due to quench, fluid inclusions and cleavage in crystals), and differential characteristics in the absorption of infrared light between the standard and specimen (*e.g.*, Moenke-Blankenburg 1989, Jackson *et al.* 1992, Jarvis *et al.* 1992, Fedorowich *et al.* 1993, Feng *et al.* 1993, Jarvis & Williams 1993, Williams & Jarvis 1993, Feng 1994, Jenner *et al.* 1993). Also, instrumental drift of the ICP-MS can affect precision and accuracy of the analysis. This drift is corrected by using an external standard for calibration (in our case, HF-13 glass, as mentioned in the above protocol).

*Proof of homogeneity of in-house standards at the trace-element level using EMPA, SXRFM, and LAM-ICP-MS*

Trace-element homogeneity of both in-house standards has been investigated by EMPA, SXRFM, and LAM-ICP-MS. The EMPA was operated at an accelerating potential of 25 kV, with a beam current of 50 nA and a beam diameter of 10  $\mu\text{m}$ . The first test was to analyze subsamples of HF-13 for Sr (concentration in HF-13: 1516 ppm). The amount of Sr in P-MT standard (469 ppm; see Table 3) is too low to give reliable counting-statistics by EMPA. The Sr $L\alpha$  line was counted for 100 s, and backgrounds on both sides for 50 s. Based on four line-profiles of 10 points each, located randomly on HF-13 subsamples, the relative standard deviation (RSD: standard deviation/average) based on 40 analyses is 3.9%. The similarity of the theoretical RSD based upon counting statistics (*i.e.*,  $\sqrt{N_{net\ counts}}/N_{net\ counts} = 4.43\%$ ) with the measured RSD suggests that the sample is homogeneous in Sr.

Other tests were performed for Rb, Sr, Y, Zr, and Nb using SXRFM and LAM-ICP-MS and Ba, La, Ce, Nd, Sm, Eu, Hf, and Ta using LAM-ICP-MS. The RSD determined on the P-MT in-house standard using both

microbeam instruments is close to or less than 10%, with the exception of Zr and Nb, as obtained by SXRFM, which display an RSD maximum of 19% (Fig. 4a). For the HF-13 in-house standard, the RSD values of all elements are close to, or below, 12% for both instruments (Fig. 4b). However, the RSD values calculated on both in-house standards for Rb, Sm, Eu, Hf, and Ta by LAM-ICP-MS are higher than that for Sr, Y, Zr, Nb, Ba, La, Ce, and Nd. One hypothesis is that these elements do not behave in a similar manner to the internal standard (in our case,  $^{44}\text{Ca}$ ) during the ablation and ionization (Williams & Jarvis 1993). The RSD values for both in-house standards have a similar pattern and similar relative values for each instrument. The low values of RSD calculated for both in-house standards show that they are homogeneous in Rb, Sr, Y, Zr, Nb, Ba, La, Ce, Nd, Sm, Eu, Hf, and Ta using the different microprobe techniques and suggest that they are probably homogeneous in other trace elements.

The upper portions of Figure 4 show the measured concentrations of Rb, Sr, Y, Zr, Nb, Ba, La, Ce, Nd, Sm, Eu, Hf, and Ta in P-MT and HF-13 using SXRFM and LAM-ICP-MS results compared to solution-mode ICP-MS analyses of the glasses (Table 3). For LAM-ICP-MS analyses, HF-13 was used for calibration. These plots are based on average values from ten-point, SXRFM, and ten-grid, LAM-ICP-MS analyses from top and middle subsamples of each glass. With the exception of Zr, trace-element concentrations in P-MT can be reproduced to within  $\pm 20\%$  by SXRFM and within  $\pm 15\%$  by LAM-ICP-MS (Fig. 4a). The concentration of Zr determined by SXRFM has a large difference relative to the working value ( $>30\%$ ). This correlates with the high RSD calculated previously (RSD of Zr: 19%), and may be explained by imperfect peak-fitting. We know that in the high-energy range of the spectra (*e.g.*, 14.5 to 17 keV), there exists a zone where many peaks overlap. A better peak-fitting routine will improve the results for these elements, but the present results are still acceptable. The trace-element concentrations of HF-13 can be reproduced well by the SXRFM technique with a relative error of  $\pm 20\%$  based on average values (Fig. 4b), with the exception of Nb determined by SXRFM, which shows a larger discrepancy,  $\sim 20\%$ . Again, better peak-fitting should improve the results. Overall, the SXRFM results are very good and compare favorably with systematic errors previously reported for this instrument,  $\pm 20\%$  relative (Lu *et al.* 1989). The accuracies associated with concentrations of Rb, Sr, Y, Zr, Nb, Ba, La, Ce, Nd, Sm, Eu, Hf, and Ta by LAM-ICP-MS on the HF-13 glass are similar to those on P-MT glass ( $\pm 10$  to 15%). In general, the LAM-ICP-MS gives better reproducibility than SXRFM for Sr, Y, Zr, and Nb. The LAM-ICP-MS has poor precision for Rb, Sm, Eu, Hf, and Ta, resulting in large standard deviations on multiple analyses (Fig. 4).

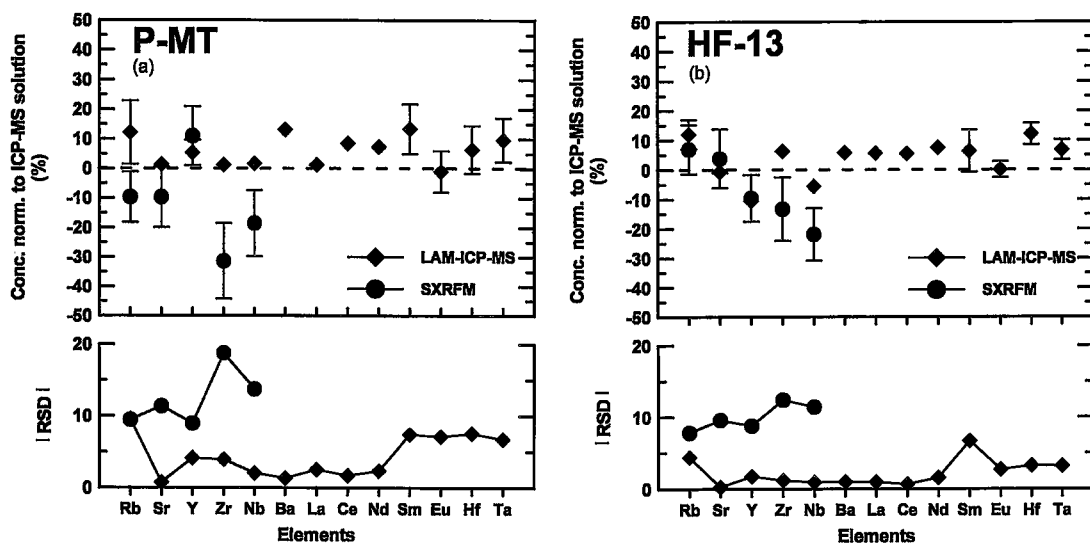


FIG. 4. SXRFM and LAM-ICP-MS results on both in-house glass standards. The concentration of each element is normalized to solution-mode ICP-MS values in Table 3. (a) P-MT standard. (b) HF-13 standard. Symbols denote: average value based on top and middle subsamples performed by LAM-ICP-MS (diamond); average value based on top and middle subsamples performed by SXRFM (circle). The error bars shown reflect  $\pm 1$  standard deviation of ten-point (SXRFM) or ten-grid (LAM-ICP-MS) analyses. Standard deviations smaller than symbol size are not shown in this and subsequent figures. The relative standard deviation (RSD in %) is calculated from the net counts and based on ten analyses, including top and middle subsamples.

Lack of matrix matching in major, minor and trace elements, variation in ablation coupling-absorption, physical features, *etc.*, cannot explain these differences for those elements because of the similarity of the in-house standard and the unknown (Jackson *et al.* 1992, Williams & Jarvis 1993). Furthermore, the Rb, Sm, Eu, Hf, and Ta isotopes determined by LAM-ICP-MS and solution ICP-MS are the same (*i.e.*,  $^{85}\text{Rb}$ ,  $^{147}\text{Sm}$ ,  $^{151}\text{Eu}$ ,  $^{178}\text{Hf}$ ,  $^{181}\text{Ta}$ ), and there is no evidence of any interferences.

#### Sensitivity and detection limits of SXRFM and LAM-ICP-MS techniques

The sensitivities of SXRFM and LAM-ICP-MS were tested using both in-house standard glasses. The purpose of this test was to verify the linear response of the SXRFM and LAM-ICP-MS to changes in the concentrations of different trace elements in our in-house glasses. Also, this test was done for the LAM-ICP-MS to determine the possibility of calibrating with a single in-house standard (in our case, HF-13) for quantitative analysis of our experimental run-products for a suite of trace elements. We define sensitivity by the relation

$$S_i = \frac{(\text{Counts}_{\text{net-}i})}{(T_{\text{live}} \times \text{Abund}_i)}$$

where  $S_i$  is the sensitivity of a particular element  $i$ ,  $\text{Counts}_{\text{net-}i}$  are the background-corrected counts for element  $i$  ( $K\alpha$  or isotope peaks for SXRFM and LAM-ICP-MS, respectively),  $T_{\text{live}}$  is the live time spent during acquisition for the element  $i$  (values of 390 s and 1.997 s were used for the SXRFM and the LAM-ICP-MS analysis, respectively), and  $\text{Abund}_i$  is the relative abundance of the isotope  $i$  analyzed with the LAM-ICP-MS [for SXRFM, this variable equals one for all the elements; abundance values taken from De Bièvre & Barnes (1985)].

The sensitivity behaves linearly for both instruments to 30 ppm for Rb, 1600 ppm for Sr, 30 ppm for Y, 300 ppm for Zr, and 120 ppm for Nb (the maximum concentrations of these elements in our in-house standards). However, a larger scatter at low count-rates has been found for all elements in P-MT glass analyzed by SXRFM compared to LAM-ICP-MS results. This reflects the lower sensitivity of the SXRFM with a small beam-spot at low concentrations, or the higher background-levels of the SXRFM compared to the LAM-ICP-MS. The overall sensi-

vity of the LAM-ICP-MS is about 1.5 to 2 orders of magnitude (*i.e.*,  $10^{1.5}$  to  $10^2$ , respectively) greater than the SXRFM for Rb, Sr, Y, Zr, and Nb.

The lower limit of detection for both instruments can be calculated following Bos *et al.* (1984) with the relation

$$LLD = 3.29 \times f \times Conc_i \times Abund_i \times \frac{(N_{bkg-i})^{1/2}}{N_{net\ peak-i}}$$

where *LLD* is the lower limit of detection, 3.29 is a constant (defined previously by Currie 1968, Eq. 5b), *f* is the correction factor for low background-counts ( $1 \leq f \leq \sqrt{2}$ ; a value of  $\sqrt{2}$  was used for both instruments by considering the propagation of the errors between the background and peak; Currie 1968), *Conc<sub>i</sub>* is the concentration of the element *i* (ppm), *Abund<sub>i</sub>* is the relative abundance of the isotope *i* quantified with the LAM-ICP-MS [for SXRFM, this variable equals one for all elements; abundance values taken from De Bièvre & Barnes (1985)], *N<sub>bkg-i</sub>* is the total number of background counts of element *i* (*Kα* or isotope peaks for SXRFM and LAM-ICP-MS, respectively), and *N<sub>net peak-i</sub>* is the total background-corrected counts of the peak of element *i* (*Kα* or the isotope peaks for SXRFM and LAM-ICP-MS, respectively).

This formula was used to calculate LLD values for SXRFM analysis and could be used for any analytical instrument (Currie 1968). However, it seems in general to overestimate the LLD calculated for LAM-ICP-MS by an average factor of 1.7 for Rb, Sr, Y, Zr, Nb, Ba, La, Ce, Nd, Sm, Eu, Hf, and Ta if compared to the relation (H. Longenrich, pers. comm., 1995):

$$LLD = 3 \times Conc_i \times Abund_i \times \frac{Std_{bkg-i}}{C_{net\ peak-i}}$$

where *Std<sub>bkg-i</sub>* is the standard deviation of the total background counts (or cps) of the element *i* (*Kα* or isotope peaks for SXRFM and LAM-ICP-MS, respectively), *C<sub>net peak-i</sub>* stands for the background-corrected counts (or cps) of the element *i* (*Kα* or isotope peaks for SXRFM and LAM-ICP-MS, respectively).

Typical lower limits of detection for Rb, Sr, Y, Zr, and Nb have been calculated for both glasses using the relation of Bos *et al.* (1984), and are listed in Table 3. The overall lower limits of detection for elements determined by SXRFM and LAM-ICP-MS are on the order of 5.5 ppm and 2 ppm or less, respectively, and are assumed to be the most conservative LLD values that could be determined for LAM-ICP-MS (Table 3). Those results are of the same order of magnitude as those reported in previous studies (Sutton *et al.* 1986, Bajt *et al.* 1992, Jackson *et al.* 1992, Williams & Jarvis 1993).

#### PARTITION COEFFICIENTS FROM RUN PRODUCTS USING SXRFM AND LAM-ICP-MS DATA

Kaersutite megacrysts from Hoover Dam, Arizona, were ground (<500 μm) and used as starting materials. Mixtures of this kaersutite powder + 10 wt% deionized water were enclosed in graphite capsules and then sealed inside Ag<sub>50</sub>Pd<sub>50</sub> capsules. Experiments were performed in a piston-cylinder apparatus with an NaCl-pyrex assembly 1.91 cm in diameter (Baker 1993, Fig. 8.10). Temperatures was measured with a type-D thermocouple, and no corrections were applied for the effect of pressure on EMF. Experiments were performed by bringing the pressure and temperature of the assembly to 1.5 GPa, 1200°C for 1 h to totally melt the amphibole. The samples then were isobarically cooled at a rate of 10°C/min to 1100°C, and that temperature was maintained for 100 h before quenching. Our previous experiments have shown that constant partition-coefficients seem to be reached within 10 h, but long-duration experiments result in larger crystals that are easier to analyze (Dalpé *et al.* 1992). Run products were inspected optically under oil, and chips of quenched glass + crystals were mounted in epoxy for analysis by EMPA, SXRFM and LAM-ICP-MS.

Run products consist of prisms of calcic amphibole (up to 1 mm along their longest axis; modal proportion: 85%) and hydrated Ti-rich quenched glass (modal proportion: 15%). The calcic amphibole is Ti-rich pargasite based on the classification of Leake (1978), and has a higher Mg number [*i.e.*, Mg# = 100Mg/(Mg+Fe) = 85] compared to the amphibole in other experimental studies [*e.g.*, Nicholls & Harris (1980): average Mg# 72; Green & Pearson (1985): Mg# 70; Adam *et al.* (1993): average Mg# 77; Adam & Green (1994): average Mg# 77, J. Adam (pers. comm., 1994): Mg# 72]. The crystal chemistry of our pargasite shows the same amount of calcium in the M4 site [<sup>VI</sup>Ca<sub>M4</sub>, normalized on a basis of 23 atoms of oxygen per formula unit (apfu)], but a higher proportion of titanium in the M1, M2 and M3 octahedral sites (<sup>VI</sup>Ti<sub>M1,2,3</sub> 0.47 apfu) compared to that found in other studies [Philpotts & Schnetzler (1970): <sup>VI</sup>Ti 0.41; Nicholls & Harris (1980): <sup>VI</sup>Ti 0.27; Green & Pearson (1985): <sup>VI</sup>Ti 0.40; Adam *et al.* (1993): <sup>VI</sup>Ti 0.23, Adam & Green (1994): <sup>VI</sup>Ti 0.23, J. Adam (pers. comm., 1994): <sup>VI</sup>Ti 0.25]. The composition of the quenched glass is listed in Table 5. It has an Mg# of 65, and contains 7 wt% normative Ne. It is a Ti-rich basanitic glass based on the classification of Yoder & Tilley (1962).

Line traverses were performed by EMPA across the pargasite and quenched glass to evaluate their homogeneity in major and trace elements (Fig. 5). The EMPA was operated at an accelerating potential of 15 kV, with a beam current of 50 nA and a beam diameter of 10 μm. The Mg profile shows two flat

TABLE 5. COMPOSITION OF PARGASITE AND QUENCHED TI-RICH BASANITIC MELT FROM RUN PRODUCTS AT 1.5 GPa, 1100 °C

| Major elements (in wt%) determined by EMPA <sup>1</sup> : |           |                     | Ti-rich hydrous basanitic quenched melt |        |  |
|---|-----------|---------------------|---|--------|--|
|   | Pargasite |                     | 17                                      |        |  |
| n   | 18        |                     |   |        |  |
| SiO <sub>2</sub>  | 41.13     | (0.42) <sup>2</sup> | 38.82                                   | (1.14) |  |
| TiO <sub>2</sub>  | 4.33      | (0.21)              | 5.67                                    | (0.26) |  |
| Al <sub>2</sub> O <sub>3</sub>                            | 14.03     | (0.43)              | 13.90                                   | (0.87) |  |
| FeO   | 5.08      | (0.25)              | 7.11                                    | (0.58) |  |
| MnO   | 0.07      | (0.02)              | 0.18                                    | (0.03) |  |
| MgO   | 16.70     | (0.19)              | 6.82                                    | (1.72) |  |
| CaO   | 11.37     | (0.37)              | 11.26                                   | (0.85) |  |
| Na <sub>2</sub> O   | 2.19      | (0.12)              | 1.70                                    | (0.28) |  |
| K <sub>2</sub> O  | 1.36      | (0.38)              | 1.07                                    | (0.43) |  |
| Total   | 96.26     |                     | 86.51                                   |        |  |

| Trace elements (in ppm) determined by <sup>3</sup> : |                           |                          |               |             |                         |   |
|--|---------------------------|--------------------------|---------------|-------------|-------------------------|---|
| n  | SXRFM                     |                          | SXRFM         |             | LAM-ICP-MS <sup>4</sup> |   |
|  | Pargasite                 |                          | Quenched melt |             | Quenched melt           |   |
|  | 5                         | 5                        | 9             | 5           | 5                       | 5 |
| Rb   | <i>B-LLD</i> <sup>5</sup> | 2.02 (0.34) <sup>2</sup> | 9.78 (1.69)   | 9.19 (0.91) |                         |   |
| Sr   | 311 (41.4) <sup>2</sup>   | 334 (4.76)               | 958 (82.8)    | 889 (2.71)  |                         |   |
| Y  | 8.80 (1.17)               | 9.61 (0.76)              | 35.9 (4.43)   | 28.8 (0.74) |                         |   |
| Zr   | 13.0 (7.26)               | 15.7 (1.18)              | 109 (9.96)    | 127 (1.43)  |                         |   |
| Nb   | <i>B-LLD</i>              | 3.19 (0.37)              | 54.7 (5.89)   | 63.7 (1.40) |                         |   |
| Ba   |                           | 115 (2.95)               |               | 415 (7.46)  |                         |   |
| La   |                           | 0.62 (0.08)              |               | 16.0 (0.25) |                         |   |
| Ce   |                           | 4.01 (0.13)              |               | 60.1 (0.82) |                         |   |
| Nd   |                           | 5.91 (0.27)              |               | 41.5 (0.79) |                         |   |
| Sm   |                           | 2.06 (0.80)              |               | 11 (0.98)   |                         |   |
| Eu   |                           | 1.20 (0.07)              |               | 3.42 (0.08) |                         |   |
| Hf   |                           | 1.38 (0.20)              |               | 4.16 (0.16) |                         |   |
| Ta   |                           | 0.27 (0.06)              |               | 3.67 (0.09) |                         |   |

| Partition coefficient values determined by: |      |                             |                          |
|---|------|-----------------------------|--------------------------|
|   | EMPA | SXRFM                       | LAM-ICP-MS               |
| Ti  | 0.76 | Rb $D_{max} = 0.30^6$       | 0.22 (0.04) <sup>7</sup> |
| K   | 1.27 | Sr 0.32 (0.05) <sup>7</sup> | 0.38 (0.01)              |
|   |      | Y 0.25 (0.04)               | 0.33 (0.03)              |
|   |      | Zr 0.12 (0.07)              | 0.12 (0.01)              |
|   |      | Nb $D_{max} = 0.09$         | 0.05 (0.01)              |
|   |      | Ba 0.28 (0.01)              | 0.029 (0.005)            |
|   |      | La 0.067 (0.002)            | 0.14 (0.01)              |
|   |      | Nd 0.19 (0.07)              | 0.35 (0.02)              |
|   |      | Eu 0.33 (0.05)              | 0.07 (0.02)              |
|   |      | Hf 0.14 (0.01)              |                          |
|   |      | Ta 0.19 (0.07)              |                          |

<sup>1</sup>: Operating conditions used: see the INTRODUCTION section.  
<sup>2</sup>: Values in parentheses are based on one standard deviation from multiple analyses (1σ).  
<sup>3</sup>: Operating conditions used: see the MICROBEAM TRACE ELEMENT ANALYSIS section.  
<sup>4</sup>: Analytical masses used are listed in Table 4.  
<sup>5</sup>: *B-LLD* = concentration Below the Lower Limit of Detection.  
<sup>6</sup>:  $D_{max}$  is obtained from: highest LLD of the element / conc. of the element in quenched melt (see Table 3 for LLD values).  
<sup>7</sup>: Values in parentheses are based on one standard deviation from the relationship: S.D. =  $[(C^2_{min} * S.D.^2_{gt} / C^4_{gt}) + (S.D.^2_{min} / C^2_{gt})]^{0.5}$  where: C = concentration; m = mineral; gt = glass (Adam *et al.* 1993).

a rapid drop is observed in Mg, which then gradually increases to a plateau (beyond 100 μm). That pattern is attributed to modification of the melt during quenching (referred as quench-modified glass). The Sr profile shows two flat patterns also separated by a quench-modified region (Fig. 5b). Sr in the quench-modified glass shows a profile reverse from that of Mg because Sr is incompatible and Mg compatible (Fig. 5). The calculated RSD values for Sr are 31 and 13.5% for pargasite crystal and quenched glass, respectively. The high RSD calculated for Sr in the pargasite is not due to inhomogeneity, but reflects low net counts and physical features such as fractures in the crystal. The RSD calculated in the quench glass for Sr and Mg are similar (<15%) and indicate homogeneity in both cases.

Concentrations of major, minor and trace elements were measured using the procedures previously described in the pargasite and quenched glass with the EMPA, SXRFM and LAM-ICP-MS (Table 5). Within one standard deviation, there is agreement for Sr, Y, and Zr in pargasite, as documented by both SXRFM and LAM-ICP-MS (Table 5). However, the concentrations of Rb and Nb are below the limit of detection for the SXRFM (<3 and 5.5 ppm, respectively; Table 3).

For the quenched glass, we report data collected 100 μm beyond the zone of quench-modified glass (Fig. 5). This is possible owing to large areas of quenched glass found in this run product (glass area of 400 × 700 μm). The level of concentration of Rb, Sr, Y, Zr, and Nb determined by SXRFM in the quenched glass lies within, or close to, one standard deviation of LAM-ICP-MS values (Table 5) and invariably within two standard deviations.

Partition coefficients (*i.e.*,  $D = C_i^{crystal} / C_i^{melt}$ ) of selected trace elements were calculated based on SXRFM (Sr, Y, Zr) and LAM-ICP-MS (Rb, Sr, Y, Zr, Nb, Ba, La, Ce, Nd, Sm, Eu, Hf, Ta) data on pargasite and quenched Ti-rich basanitic glass (Table 5). The partition coefficients  $D_{Sr}$ ,  $D_{Zr}$ , and  $D_Y$  measured by SXRFM between the crystal and the quenched glass are within two standard deviations of values derived from the LAM-ICP-MS data (Table 5).

The partition coefficients  $D_{Ba}$ ,  $D_{Rb}$ ,  $D_{Ta}$ ,  $D_{Nb}$ ,  $D_{La}$ ,  $D_{Sr}$ ,  $D_{Zr}$ , and  $D_Y$  measured by both techniques agree well with previous experimental results, with the exception of  $D_{Sm}$ , which is lower than the values measured by Nicholls & Harris (1980), Green & Pearson (1985), Adam *et al.* (1993), Adam & Green (1994), and J. Adam (pers. comm., 1994) (Fig. 6a). Our new values for  $D_{Ce}$ ,  $D_{Nd}$ ,  $D_{Hf}$ , and  $D_{Eu}$  determined from LAM-ICP-MS data agree well with the interpolated fields that are formed by previous experimental results (Fig. 6a). In general, our partition coefficients are lower than partition coefficients measured between natural pargasite and coexisting matrix (Higuchi & Nagasawa 1969, Philpotts & Schnetzler 1970,

patterns, one from core to rim in the pargasite crystal and a second located about 100 μm away from the rim (referred to the quenched glass) (Fig. 5a). RSD factors of 1.3 and 12.6% were calculated for the two phases, respectively. Some peaks and troughs along the crystal profile are related to fractures made during the polishing and to cleavage in the thin crystal. As we cross from the rim of the crystal to the quenched glass,

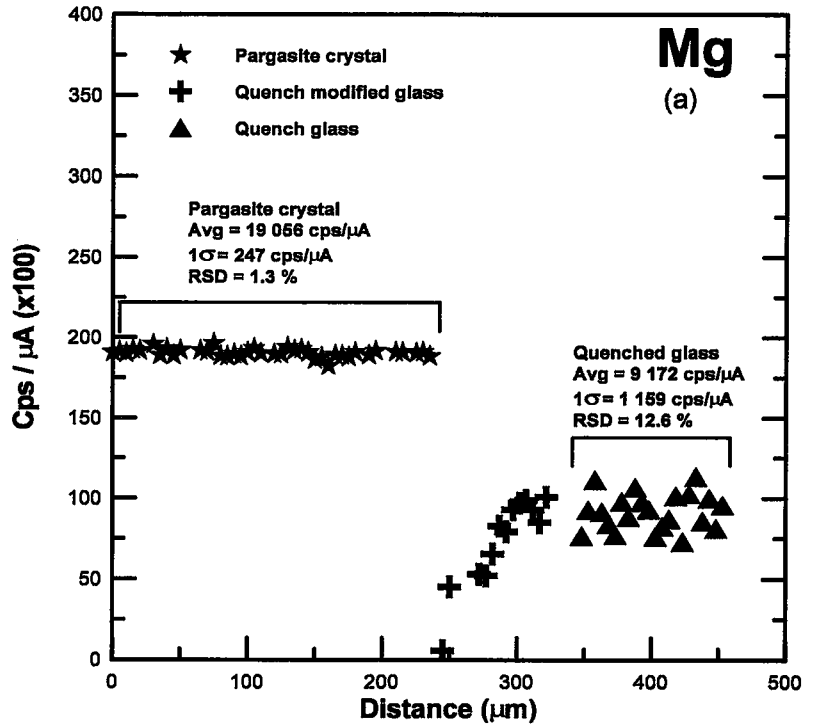
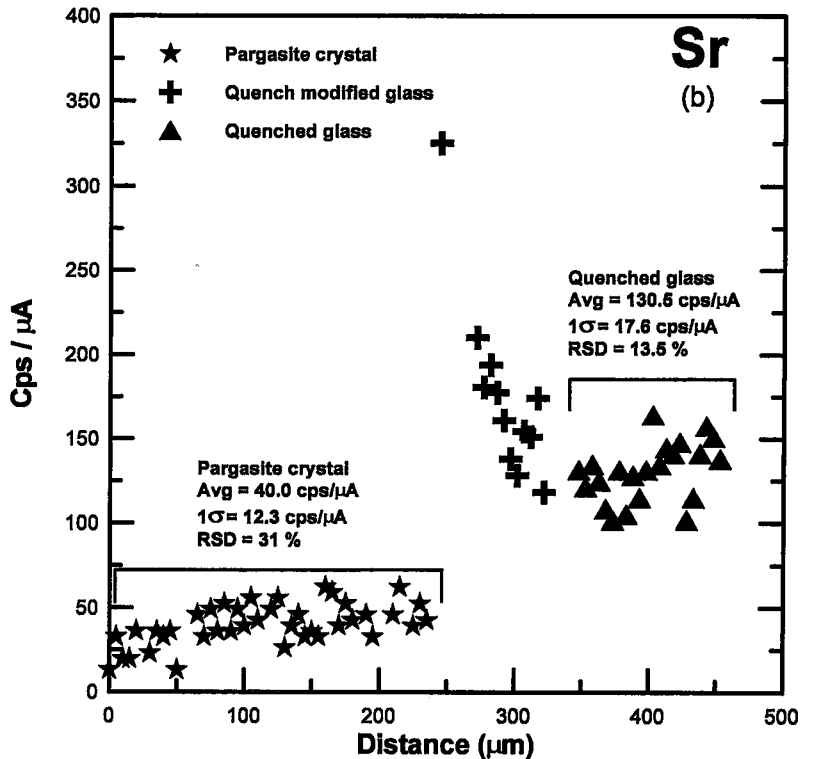


FIG. 5. Line traverse showing results of background-corrected qualitative analyses by EMPA on BD1008 run products. (a) Mg; (b) Sr. Symbols denote: pargasite crystal (star); quench-modified glass close to rim (cross); quenched glass located at >100 μm from rim position (triangle).



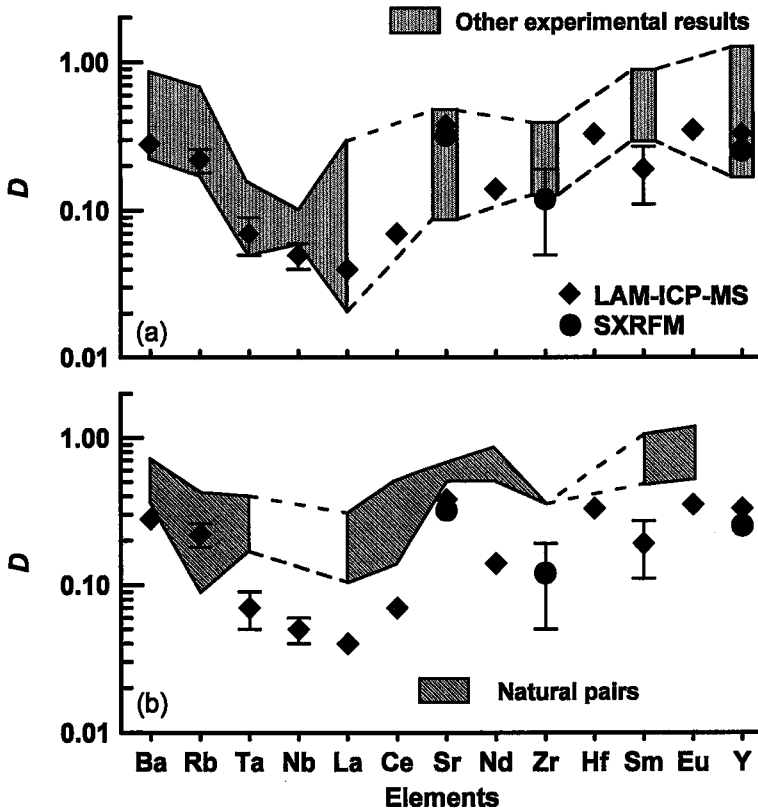


FIG. 6. Partition coefficients determined by SXRFM and LAM-ICP-MS between pargasite and Ti-rich basanitic quenched melt. (a) Experimental run-products. Symbols denote: SXRFM (circle); LAM-ICP-MS (diamond); other experimental results [sources: Nicholls & Harris (1980), Green & Pearson (1985), Adam *et al.* (1993), Adam & Green (1994), J. Adam (pers. comm., 1994)]. The error bars shown reflect one standard deviation from the relationship:  $S.D. = [(C_m^2 * S.D._m^2 / C_{gl}^4) + (S.D._m^2 / C_{gl}^2)]^{0.5}$ , where  $C$  represents concentration,  $m$  stands for mineral, and  $gl$  stands for glass (Adam *et al.* 1993). (b) Natural pairs showing minimum and maximum partition-coefficients between pargasite and host rocks [sources: Higuchi & Nagasawa (1969), Philpotts & Schnetzler (1970), Nagasawa (1973), Sun & Hanson (1976), Irving & Price (1981), Liotard *et al.* (1983) and Lemarchand *et al.* (1987)].

Nagasawa 1973, Sun & Hanson 1976, Irving & Price 1981, Liotard *et al.* 1983, Lemarchand *et al.* 1987) (Fig. 6b). Such discrepancies between natural and experimental studies are well documented and may suggest disequilibrium in the case of natural pairs (Green & Pearson 1985, Beattie 1994).

Partition coefficients for the REE determined in this study are low compared to those documented in most other studies (Fig. 6a). The glass compositions of these earlier experimental studies range from basanitic to tholeiitic and do not demonstrate any obvious effects of composition on the partition coefficients. However, it is possible that slight differences in amphibole composition (perhaps differ-

ences in  $^{VI}Ti_{M1,2,3}$  in the pargasitic run-products, as mentioned previously) have a significant effect on the partition coefficients of trivalent elements. Adam & Green (1994) noted that for amphibole and clinopyroxene, there is a linear relationship between partition coefficients for Ti and the REE; as  $D_{Ti}$  increases,  $D$  values for the REE increase at constant pressure and temperature. The low partition-coefficients for Ti and the REE measured in this study are qualitatively consistent with the results of Adam & Green (1994). However, the influence of the structure of pargasite and the quantitative relationships between REE partition coefficients and Ti cannot be established more firmly without more experiments.

COMPARISON OF SXRFM AND LAM-ICP-MS,  
AND CONCLUSIONS

The two analytical techniques are reliable and convenient techniques for the quantitative determination of the level of concentration of trace elements. The SXRFM offers the possibility of analyzing silicates for all elements between chlorine and molybdenum using  $K\alpha$  lines (2.822 to 20 keV) at a very small spatial resolution (on the order of tens of  $\mu\text{m}$ ) without specimen damage. The LAM-ICP-MS offers the possibility of analyzing a larger suite of elements (e.g., from mass  $^7\text{Li}$  to  $^{238}\text{U}$ ) at lower limits of detection than the SXRFM, but damages the sample during analysis.

The overall lower limit of detection for Rb, Sr, Y, Zr, and Nb is on the order of 5.5 ppm and 2 ppm, respectively, for SXRFM and LAM-ICP-MS techniques; the techniques can reproduce the concentrations of these elements within  $\pm 20\%$  and  $\pm 15\%$  of the accepted values, respectively. However, the LAM-ICP-MS data reveal irregular precision in the Rb, Sm, Eu, Hf, and Ta concentrations, which we attribute to the different behaviors of Rb, Sm, Eu, Hf, and Ta relative to the internal standard,  $^{44}\text{Ca}$ , during ablation. Furthermore, the larger area sampled by the LAM-ICP-MS limits this instrument to use on specimens that are homogeneous at the scale of hundreds of  $\mu\text{m}$ . Future development of LAM-ICP-MS should allow a significant decrease in this size.

Both instruments were used to measure the partition coefficients (i.e.,  $D = C_i^{\text{crystal}}/C_i^{\text{melt}}$ ) between pargasite and a Ti-rich basanitic quenched melt on the same run-products. Similar values of  $D_{\text{Sr}}$  and  $D_{\text{Y}}$ , and identical values of  $D_{\text{Zr}}$ , were measured by both instruments. Also, these  $D$  values, together with  $D_{\text{Ba}}$ ,  $D_{\text{Rb}}$ ,  $D_{\text{Ta}}$ ,  $D_{\text{Nb}}$ ,  $D_{\text{La}}$  measured by LAM-ICP-MS, agree well with published results of experimental studies. New values of  $D_{\text{Ce}}$ ,  $D_{\text{Nd}}$ ,  $D_{\text{Hf}}$ , and  $D_{\text{Eu}}$  from experimental results in a basaltic system are reported here for the first time.

ACKNOWLEDGEMENTS

C. Dalpé personally thanks his wife Renée for her encouragement until her last minute in our world. We thank Mark Rivers, Saša Bajt and Pat Nuessle (Brookhaven National Laboratory) for providing technical assistance with SXRFM on X26A. G. Gauthier and A. Khoury (both at Université de Montréal) are thanked for providing support on the LAM-ICP-MS. D. Francis graciously furnished HF-13 rock powder and its bulk composition. Tom Skulski is thanked for constructive comments during CD's introduction to the SXRFM. We thank Trevor H. Green, D. Günther, L. Forsythe, George Jenner, Robert F. Martin, John Stix, and Henry Longerich for their constructive comments, which greatly improved the manuscript. This research was supported by a NSERC scholarship to C. Dalpé, NSERC grant OGP89662 and FCAR

Nouveau Chercheur Grant to D.R. Baker, and DOE DE#-FG02-92ER14244, NASA NAG9-106, NSF EAR89-15699 grants to S.R. Sutton.

REFERENCES

- ADAM, J. & GREEN, T.H. (1994): The effects of pressure and temperature on the partitioning of Ti, Sr and REE between amphibole, clinopyroxene and basanitic melts. *Chem. Geol.* **117**, 219-233.
- \_\_\_\_\_, \_\_\_\_\_ & SIE, S.H. (1993): Proton microprobe determined partitioning of Rb, Sr, Ba, Y, Zr, Nb and Ta between experimentally produced amphiboles and silicate melts with variable F content. *Chem. Geol.* **109**, 29-49.
- ALLÈGRE, C.J. & MINSTER, J.F. (1978): Quantitative models of trace element behavior in magmatic processes. *Earth Planet. Sci. Lett.* **38**, 1-25.
- \_\_\_\_\_, TREUIL, M., MINSTER, J.-F., MINSTER, B. & ALBARÈDE, F. (1977): Systematic use of trace element in igneous process. I. Fractional crystallization processes in volcanic suites. *Contrib. Mineral. Petrol.* **60**, 57-75.
- BAJT, S., RIVERS, M. & SUTTON, S. (1992): X-ray fluorescence microprobe. In Workshop on Applications of Synchrotron Radiation to Earth Materials. National Synchrotron Light Source, Brookhaven National Laboratory, Upton, N.Y.
- BAKER, D.R. (1993): Measurement of diffusion at high temperatures and pressures in silicate systems. In Experiments at High Pressure and Applications to the Earth's Mantle (R.W. Luth, ed.). *Mineral. Assoc. Can., Short-Course Handbook* **21**, 305-355.
- BEATTIE, P. (1994): Systematics and energetics of trace-element partitioning between olivine and silicate melts: implication for the nature of mineral/melt partitioning. *Chem. Geol.* **117**, 57-71.
- BOS, A.J.J., VIS, R.D., VERHEUL, H., PRINS, M., DAVIES, S.T., BOWEN, D.K., MAKJANIĆ, J. & VALKOVIĆ, V. (1984): Experimental comparison of synchrotron radiation with other modes of excitation of X rays for trace element analysis. *Nucl. Instrum. Methods Phys. Res.* **B3**, 232-240.
- BOTTINGA, Y., WEILL, D. & RICHER, P. (1982): Density calculations for silicate liquids. I. Revised method for aluminosilicate compositions. *Geochim. Cosmochim. Acta* **46**, 909-919.
- BOYD, F.R. & FINGER, L.W. (1975): Homogeneity of minerals in mantle rocks from Lesotho. *Carnegie Inst. Wash. Yearbook* **74**, 519-525.
- CAMPBELL, I. & SCHENK, E.T. (1950): Camptonite dikes near Boulder Dam, Arizona. *Am. Mineral.* **35**, 671-692.
- CHEATHAM, M.M., SANGREY, W.F. & WHITE, W.M. (1993): Sources of error in external calibration ICP-MS analysis of geological samples and an improved non-linear drift correction procedure. *Spectrochim. Acta* **48B**, E487-E506.

- CURRIE, L.A. (1968): Limits for qualitative detection and quantitative determination. *Anal. Chem.* **40**, 586-593.
- DALPÉ, C. & BAKER, D.R. (1994a): Partition coefficients for rare-earth elements between calcic amphibole and Ti-rich basanitic glass at 1.5 GPa, 1100°C. *Mineral. Mag.* **58A**, 207-208.
- & ————— (1994b): Pargasite – basanitic melt partition coefficients determined by laser-ablation ICP-MS. *Eos (Trans. Am. Geophys. Union)* **75**, 372 (abstr.).
- , ————— & SUTTON S.R. (1992): Partition coefficient of Ti, Cr, Ga, Rb, Sr, Y, Nb, and Zr between pargasite and nephelinitic melt at 1.5 GPa. *Eos (Trans. Am. Geophys. Union)* **73**, 607 (abstr.).
- DE BIÈVRE, P. & BARNES, I.L. (1985): Table of the isotopic composition of the elements as determined by mass spectrometry. *Int. J. Mass Spectrom. Ion Proc.* **65**, 211-230.
- DEER, W.A., HOWIE, R.A. & ZUSSMAN, J. (1985): *An Introduction to the Rock-Forming Minerals*. Longman, London, U.K.
- FEDEROWICH, J.S., RICHARDS, J.P., JAIN, J.C., KERRICH, R. & FAN, J. (1993): A rapid method for REE and trace-element analysis using laser sampling ICP-MS on direct fusion whole-rock glasses. *Chem. Geol.* **106**, 229-249.
- FENG, RUI (1994): In situ trace element determination of carbonates by laserprobe inductively coupled plasma mass spectrometry using nonmatrix matched standardization. *Geochim. Cosmochim. Acta* **58**, 1615-1623.
- , MACHADO, N. & LUDDEN, J. (1993): Lead geochronology of zircon by laserprobe – inductively coupled plasma mass spectrometry (LP-ICPMS). *Geochim. Cosmochim. Acta* **57**, 3479-3486.
- FRANCIS, D. & LUDDEN, J. (1995): The signature of amphibole in mafic alkaline lavas, a study in the northern Canadian Cordillera. *J. Petrol.* **36** (in press).
- GORDON, B.M. (1982): Sensitivity calculations for multi-elemental trace analysis by synchrotron radiation induced X-ray fluorescence. *Nucl. Instrum. Methods Phys. Res.* **204**, 223-229.
- GOVINDARAJU, K. (1989): 1989 Compilation of working values and sample description for 272 geostandards. *Geostand. Newslett.* **13**, 1-113.
- GREEN, T.H. (1994): Experimental studies of trace-element partitioning applicable to igneous petrogenesis – Sedona 16 years later. *Chem. Geol.* **117**, 1-36.
- & PEARSON, N.J. (1985): Experimental determination of REE partition coefficients between amphibole and basaltic to andesitic liquids at high pressure. *Geochim. Cosmochim. Acta* **49**, 1465-1468.
- HAWTHORNE, F.C. (1993): Minerals, mineralogy and mineralogists: past, present and future. *Can. Mineral.* **31**, 253-296.
- HICKSON, C.J. & JURAS, S.J. (1986): Sample contamination by grinding. *Can. Mineral.* **24**, 585-589.
- HIGUCHI, H. & NAGASAWA, H. (1969): Partition of trace elements between rock-forming minerals and the host volcanic rocks. *Earth Planet. Sci. Lett.* **7**, 281-287.
- HOFMANN, A.W. (1986): Nb in Hawaiian magmas: constraints on source composition and evolution. *Chem. Geol.* **57**, 17-30.
- IRVING, A.J. & PRICE, R.C. (1981): Geochemistry and evolution of lherzolite-bearing phonolitic lavas from Nigeria, Australia, East Germany and New Zealand. *Geochim. Cosmochim. Acta* **45**, 1309-1320.
- JACKSON, S.E., LONGERICH, H.P., DUNNING, G.R. & FRYER, B.J. (1992): The application of laser-ablation microprobe – inductively coupled plasma – mass spectrometry (LAM-ICP-MS) to *in situ* trace-element determinations in minerals. *Can. Mineral.* **30**, 1049-1064.
- JARVIS, K.E., GRAY, A.L. & HOUK, R.S. (1992): *Handbook of Inductively Coupled Plasma Mass Spectrometry*. Blackie, Glasgow, U.K.
- & WILLIAMS, J.G. (1993): Laser ablation inductively coupled plasma mass spectrometry (LA-ICP-MS): a rapid technique for the direct, quantitative determination of major, trace and rare-earth elements in geological samples. *Chem. Geol.* **106**, 251-262.
- JENNER, G.A., FOLEY, S.F., JACKSON, S.E., GREEN, T.H., FRYER, B.J. & LONGERICH, H.P. (1993): Determination of partition coefficients for trace elements in high pressure – temperature experimental run products by laser ablation microprobe – inductively coupled plasma – mass spectrometry (LAM-ICP-MS). *Geochim. Cosmochim. Acta* **57**, 5099-5103.
- , LONGERICH, H.P., JACKSON, S.E. & FRYER, B.J. (1990): ICP-MS – a powerful tool for high-precision trace-element analysis in earth sciences: evidence from analysis of selected U.S.G.S. reference samples. *Chem. Geol.* **83**, 133-148.
- JONES, K.W., GORDON, B.M., HANSON, A.L., HASTINGS, J.B., HOWELLS, M.R., KRANER, H.W. & CHEN, J.R. (1984): Application of synchrotron radiation to elemental analysis. *Nucl. Instrum. Methods Phys. Res.* **B3**, 225-231.
- KRESS, V.C. & CARMICHAEL, I.S.E. (1991): The compressibility of silicate liquids containing Fe<sub>2</sub>O<sub>3</sub> and the effect of composition, temperature, oxygen fugacity and pressure on their redox states. *Contrib. Mineral. Petrol.* **108**, 82-92.
- LEAKE, B.E. (1978): Nomenclature of amphiboles. *Am. Mineral.* **63**, 1023-1052.

- LEMARCHAND, F., VILLEMANT, B. & CALAS, G. (1987): Trace element distribution coefficients in alkaline series. *Geochim. Cosmochim. Acta* **51**, 1071-1081.
- LIOTARD, J.-M., BOIVIN, P., CANTAGREL, J.-M., & DUPUY, C. (1983): Mégacristaux d'amphibole et basaltes alcalins associés. Problèmes de leurs relations pétrogénétiques et géochimiques. *Bull. Minéral.* **106**, 451-464.
- LONGERICH, H.P., JENNER, G.A., FRYER, B.J. & JACKSON, S.E. (1990): Inductively coupled plasma – mass spectrometric analysis of geological samples: a critical evaluation based on case studies. *Chem. Geol.* **83**, 105-118.
- LU, FANG-QIONG, SMITH, J.V., SUTTON, S.R., RIVERS, M.L. & DAVIS, A.M. (1989): Synchrotron x-ray fluorescence analysis of rock-forming minerals. 1. Comparison with other techniques. 2. White-beam energy-dispersive procedure for feldspars. *Chem. Geol.* **75**, 123-143.
- MOENKE-BLANKENBURG, L. (1989): Laser microanalysis. In *Chemical Analysis 105* (J.D. Winefordner, ed.). Wiley-Interscience, New York, N.Y.
- NAGASAWA, H. (1973): Rare-earth distribution alkali rocks from Oki-Dogo Island, Japan. *Contrib. Mineral. Petrol.* **39**, 301-308.
- NICHOLLS, I.A. & HARRIS, K.L. (1980): Experimental rare earth element partition coefficients for garnet, clinopyroxene and amphibole coexisting with andesitic and basaltic liquids. *Geochim. Cosmochim. Acta* **44**, 287-308.
- PEARCE, N.J.G., WILLIAM, T.P., ABELL, I., DULLER, G.A.T. & FUGE, R. (1992): Mineral microanalysis by laser ablation inductively coupled plasma mass spectrometry. *J. Anal. At. Spectrom.* **7**, 53-57.
- PERKINS, W.T., PEARCE, N.J.G. & JEFFRIES, T.E. (1993): Laser ablation inductively coupled plasma mass spectrometry: a new technique for the determination of trace and ultra-trace elements in silicates. *Geochim. Cosmochim. Acta* **57**, 475-482.
- PHILPOTTS, J.A. & SCHNETZLER, C.C. (1970): Phenocryst – matrix partition coefficients for K, Rb, Sr and Ba, with applications to anorthosite and basalt genesis. *Geochim. Cosmochim. Acta* **34**, 307-322.
- SKULSKI, T., MINARIK, W. & WATSON, E.B. (1994): High-pressure experimental trace-element partitioning between clinopyroxene and basaltic melts. *Chem. Geol.* **117**, 127-148.
- SUN, SHEN-SU & HANSON, G.N. (1976): Rare earth element evidence for differentiation of McMurdo Volcanics, Ross Island, Antarctica. *Contrib. Mineral. Petrol.* **54**, 139-155.
- SUTTON, S.R., DELANEY, J.S., SMITH, J.V. & PRINZ, M. (1987): Copper and nickel partitioning in iron meteorites. *Geochim. Cosmochim. Acta* **51**, 2653-2662.
- \_\_\_\_\_, RIVERS, M.L. & SMITH, J.V. (1986): Synchrotron X-ray fluorescence: diffraction interference. *Anal. Chem.* **58**, 2167-2171.
- WALLACE, R.C. (1977): Anorthoclase–calcite rodding within a kaersutite xenocryst from the Kakanui mineral breccia, New Zealand. *Am. Mineral.* **62**, 1038-1041.
- WATSON, E.B., OTHMAN, D.B., LUCK, J.-M. & HOFMANN, A.W. (1987): Partitioning of U, Pb, Cs, Yb, Hf, Re and Os between chromian diopsidic pyroxene and haplobasaltic liquid. *Chem. Geol.* **62**, 191-208.
- WILLIAMS, J.G. & JARVIS, K.E. (1993): Preliminary assessment of laser ablation inductively coupled plasma mass spectrometry for quantitative multi-element determination in silicates. *J. Anal. At. Spectrom.* **8**, 25-34.
- YODER, H.S. & TILLEY, C.E. (1962): Origin of basalt magmas: an experimental study of natural and synthetic rock systems. *J. Petrol.* **3**, 342-532.

Received October 13, 1994, revised manuscript accepted March 17, 1995.